UNIVERSITY OF LEEDS

This is a repository copy of *Tissue-specific dysregulation of mitochondrial respiratory capacity and coupling control in colon-26 tumor-induced cachexia*.

White Rose Research Online URL for this paper:
http://eprints.whiterose.ac.uk/145541/

Version: Accepted Version

Article:
Halle, JL, Pena, GS, Paez, HG et al. (5 more authors) (Cover date: 1st July 2019) Tissue-specific dysregulation of mitochondrial respiratory capacity and coupling control in colon-26 tumor-induced cachexia. AJP - Regulatory, Integrative and Comparative Physiology, 317 (1). R68-R82. ISSN 0363-6119

https://doi.org/10.1152/ajpregu.00028.2019

© 2019, the American Physiological Society. This is an author produced version of a paper published in American Journal of Physiology-Regulatory, Integrative and Comparative Physiology. Uploaded in accordance with the publisher's self-archiving policy.

Reuse
Items deposited in White Rose Research Online are protected by copyright, with all rights reserved unless indicated otherwise. They may be downloaded and/or printed for private study, or other acts as permitted by national copyright laws. The publisher or other rights holders may allow further reproduction and re-use of the full text version. This is indicated by the licence information on the White Rose Research Online record for the item.

Takedown
If you consider content in White Rose Research Online to be in breach of UK law, please notify us by emailing eprints@whiterose.ac.uk including the URL of the record and the reason for the withdrawal request.

White Rose university consortium
Universities of Leeds, Sheffield & York

eprints@whiterose.ac.uk
https://eprints.whiterose.ac.uk/

Tissue-specific dysregulation of mitochondrial respiratory capacity and coupling control in colon-26 tumor-induced cachexia

Jessica L. Halle[1], Gabriel S. Pena[1, #], Hector G. Paez[1, #], Adrianna J. Castro[1], Harry B. Rossiter[2,3], Nishant P. Visavadiya[1], Michael A. Whitehurst[1], and Andy V. Khamoui[1,4,5*]

[#]Contributed equally

[1]Department of Exercise Science and Health Promotion, Florida Atlantic University, Boca Raton, FL 33431, USA; [2]Division of Respiratory and Critical Care Physiology and Medicine, Department of Medicine, Los Angeles Biomedical Research Institute at Harbor-UCLA Medical Center, Torrance, CA 90502, USA; [3]Faculty of Biological Sciences, University of Leeds, Leeds, LS2 9JT, UK; [4]Institute for Healthy Aging and Lifespan Studies, Florida Atlantic University, Boca Raton, FL 33431, USA; [5]Cancer Research Group, Florida Atlantic University, Boca Raton, FL 33431, USA

Running Head: Tissue-specific mitochondrial function in cancer cachexia

*Address for Correspondence

Andy V. Khamoui PhD

Department of Exercise Science and Health Promotion

Florida Atlantic University

777 Glades Rd, FH-11A, Rm 128-B

Boca Raton, FL 33431

Tel: (561) 297-4450 | Email: akhamoui@fau.edu

Abstract

In addition to skeletal muscle dysfunction, cancer cachexia is a systemic disease involving remodeling of non-muscle organs such as adipose and liver. Impairment of mitochondrial function is associated with multiple chronic diseases. The tissue-specific control of mitochondrial function in cancer cachexia is not well-defined. This study determined mitochondrial respiratory capacity and coupling control of skeletal muscle, white adipose tissue (WAT), and liver in colon-26 (C26) tumor-induced cachexia. Tissues were collected from PBS-injected weight-stable mice, C26 weight-stable mice, and C26 mice with moderate (10% weight loss) and severe cachexia (20% weight loss). The respiratory control ratio (RCR, an index of OXPHOS coupling efficiency) was low in WAT during the induction of cachexia, due to high non-phosphorylating LEAK respiration. Liver RCR was low in C26 weight-stable and moderately cachexic mice due to reduced OXPHOS. Liver RCR was further reduced with severe cachexia, where Ant2 but not Ucp2 expression was increased. Ant2 was inversely correlated with RCR in the liver ($r=-0.547$, $p<0.01$). Liver cardiolipin increased in moderate and severe cachexia, suggesting this early event may also contribute to mitochondrial uncoupling. Impaired skeletal muscle mitochondrial respiration occurred predominantly in severe cachexia, at complex I. These findings suggest that mitochondrial function is subject to tissue-specific control during cancer cachexia, whereby remodeling in WAT and liver arise early and may contribute to altered energy balance, followed by impaired skeletal muscle respiration. We highlight an under-recognized role of liver and WAT mitochondrial function in cancer cachexia, and suggest mitochondrial function of multiple tissues to be therapeutic targets.

Keywords: skeletal muscle atrophy, liver, adipose, cancer cachexia, OXPHOS, high-resolution respirometry

Introduction

Approximately half of all cancer patients undergo cachexia, a life-threatening comorbidity of cancer in which tumor-induced metabolic abnormalities contribute to hallmark clinical features such as involuntary weight loss and skeletal muscle atrophy (45, 58). Despite impairing responsiveness to anti-cancer treatment and accounting for an estimated 20% of all cancer-related deaths (30), cachexia continues to be an under-recognized issue in cancer care, and a major source of frustration for patients and family members alike (50, 58). Because the root causes of cancer cachexia are not well-defined at present, effective treatment options remain elusive (22). While research efforts often emphasize skeletal muscle pathophysiology, current frameworks describe a systemic condition in which multiple organs such as adipose, bone, brain, heart, and liver are remodeled to generate the cachectic phenotype (2, 45, 46). Convincing evidence supports the existence of cross-talk mechanisms between several of these organs, and targeted manipulation of non-muscle organs rescue losses of body weight and muscle mass (34, 35). The multi-organ involvement underscores the highly complex nature of cancer cachexia, whereby multiple mechanisms of metabolic disturbance may be responsible for the hallmark clinical manifestations.

Several lines of evidence implicate mitochondria in the pathogenesis of cancer cachexia (3, 13). Mitochondria are well known for their central role in cellular function due to their regulation of nutrient oxidation and bioenergetics, diverse signaling pathways, and cell fate decisions (40). Given these critical roles, disturbances to mitochondria and their metabolic functions are implicated in aging, neurodegenerative disease, and cancer (1, 5, 6, 49). In particular, effects on mitochondrial respiration are important because oxidative phosphorylation (OXPHOS), which couples the electron transfer system (ETS) to ADP phosphorylation, can affect redox status, oxidative stress, mitochondrial dynamics, quality control, and hence the overall health of the mitochondrial pool (40). In cancer cachexia, mitochondrial function is most widely studied in skeletal muscle, with several mechanisms proposed to link mitochondrial functions to muscle mass. Elevated oxidant emission could lead to protein degradation and muscle atrophy (39, 52). Further, restricted ATP provision from impaired OXPHOS may cause energetic stress, downstream activation of protein degradation, and muscle dysfunction (16, 52). Indeed, recent reports found decreased complex I-linked OXPHOS capacity and coupling efficiency *in situ*, and reduced coupling efficiency *in vivo* in skeletal muscle of rodents with cancer cachexia (10, 23, 55). These defects were observed at or near time-points at which marked cachexia already occurred,

and are suggestive of muscle dysfunction secondary to global changes in systemic metabolism (27). The coupling and function of skeletal muscle respiration throughout the development of cancer cachexia, from early to late stage, requires further investigation.

In addition to skeletal muscle oxidative metabolism, considerable interest has been devoted to adipose tissue function as a cause of cachexia. White adipose tissue depots undergo a phenotypic switch to resemble the more metabolically active, mitochondrial-dense, heat producing brown adipose compartment (i.e. WAT beiging/browning) (35, 44). In other conditions characterized by severe metabolic stress and beiging (i.e. burn injury), WAT shows high LEAK respiration (53), which reflects the permeability of the mitochondrial inner membrane to inward electron flow and intrinsic uncoupling, thereby generating heat independent of ATP synthase activity due to compensation for the dissipation of the proton gradient. The metabolic rewiring of WAT has been proposed as a source of elevated energy expenditure and thus involuntary weight loss (44, 53). It has also been suggested that inefficiency of OXPHOS and uncoupling in the liver could be another mechanism by which energy is dissipated as heat, metabolic rate increases, and weight loss ensues (20, 46). It is not well-established, however, if mitochondrial defects in liver are part of cancer cachexia severity.

How mitochondrial respiration functions in skeletal muscle, WAT, and liver before overt features of cachexia occur, along with the extent to which they change as severe cachexia arises, is not known. This investigation tested the hypotheses that mitochondrial respiration is subject to tissue-specific control mechanisms during the induction and progression of cancer cachexia, and that these indices of mitochondrial function relate to body weight loss and skeletal muscle atrophy, the hallmark features of cancer cachexia. To address this, we assessed mitochondrial respiratory function by high-resolution respirometry during the induction and progression of cancer cachexia using the colon-26 (C26) tumor-bearing mouse model.

Methods

Animals and design

Ten-week old Balb/c males (Envigo) were randomly assigned to receive either an injection of PBS or colon-26 (C26) tumor cells. The C26 tumor-bearing mouse is a well-established pre-clinical model of cancer cachexia (4, 18, 19, 33, 42, 61). In this model the salient features of cachexia develop (i.e. weight loss, muscle atrophy) over a typical tumor growth period of 3 weeks. Tissue was collected from C26 mice between day 14

and 21 after tumor cell injection based on weight loss, followed by evaluation of mitochondrial function in groups stratified by cachexia severity according to the degree of weight loss, similar to previous investigations (7, 59). The 4 groups studied included: 1) Tumor-free, weight-stable mice that were PBS injected (PBS-WS, n=4), 2) C26 mice with confirmed tumors that did not exhibit weight loss (weight-stable, C26-WS, n=6), 3) C26 mice with moderate cachexia (10% weight loss; C26-MOD, n=7), and 4) C26 mice with severe cachexia (≥20% weight loss; C26-SEV, n=6). These classifications were adapted from prior pre-clinical investigations in which 10% weight loss was considered moderate cachexia, and 20% severe (7, 59). Weight loss for each mouse was calculated as the percentage change between carcass weight (i.e. tumor-free body weight) and body weight recorded on the day of cell injection. For all C26-SEV mice, tissue was collected on day 21 post-injection. For C26-MOD, tissue was collected on day 14 (n=4), 15 (n=1), 17 (n=1), or 21 (n=1). For the C26-WS group, tissue was collected on day 14 (n=1), 20 (n=2), or 21 (n=3). Mice were individually housed, provided food and water *ad libitum*, and maintained on a 12:12 hr light:dark cycle. C26 tumor-bearing mice may or may not exhibit anorexia depending on the source of the C26 cells and the phenotype they induce (42). The C26 cells in the present study were obtained from a cell bank that others have used to show no significant anorexia as a result of C26 tumor-induced cachexia (4). All procedures were approved by the Institutional Animal Care and Use Committee at Florida Atlantic University (Protocol # A16-39).

C26 tumor cell culture and injection

C26 cells (CLS Cell Lines Service, Eppelheim, Germany) were cultured in a humidified 5% CO_2 incubator using complete media that contained RPMI 1640 supplemented with 1% penicillin/streptomycin (vol/vol) and 10% FBS (vol/vol). Media was replaced every two to three days. At sub-confluency, cells were harvested by incubation with trypsin (0.05%, Gibco) and subsequently pelleted by centrifugation. The supernatant was then discarded and the pellet resuspended in sterile PBS. Viable cells were counted in a hemocytometer by trypan blue staining and light microscopy. Mice in C26 groups were gently restrained and injected s.c. in the upper back with a cell suspension containing 1 x 10^6 cells. Mice assigned to weight-stable control were injected with an equivalent volume of sterile PBS (19, 60).

Tissue collection and processing

Mice were euthanized by ketamine/xylazine overdose delivered i.p. (300/30 mg/kg). Euthanasia was performed during a four-hour time window from 10:00 am to 2:00 pm to ensure consistency in the timing of tissue collection. Mice were not food deprived overnight or immediately prior to tissue collection. Hindlimb skeletal muscles, vital organs, and epididymal white adipose tissue (WAT) were carefully isolated and removed. The left medial gastrocnemius, left epididymal WAT, and left lateral lobe of the liver, were immediately placed into ice-cold preservation buffer (BIOPS: 2.77 mM CaK_2EGTA, 7.23 mM K_2EGTA, 5.77 mM Na_2ATP, 6.56 mM $MgCl_2 \cdot 6H_2O$, 20 mM Taurine, 15 mM Na_2PCr, 20 mM Imidazole, 0.5 mM DTT, 50 mM MES hydrate) and stored on ice in preparation for *in situ* analysis of mitochondrial respiration. The gastrocnemius was selected because it is a major locomotor muscle that atrophies in this model (33), and has been previously used to investigate mitochondrial respiration in mouse studies of metabolic dysfunction (38, 41). Epididymal WAT was selected due to its anticipated remodeling and relative abundance, which ensured adequate tissue availability for the respirometric assay. WAT was not detectable in severe cachexia, and was therefore not analyzed in the C26-SEV group. The left lateral lobe of the liver was chosen in accordance with Heim et al (28). The right hind limb muscles were mounted cross-sectionally in tragacanth gum on cork, and frozen in isopentane cooled by liquid nitrogen for histological analysis. Remaining tissues were snap frozen and stored at -80°C.

To prepare WAT for respirometry, a portion of tissue was gently blotted dry, and two samples were prepared that weighed ~20-50 mg. Samples were sectioned into 2-3 pieces prior to placement into the two respirometer chambers. Chemical permeabilization of WAT by addition of digitonin into the chambers was not performed based on preliminary tests and reports by others in which no effect on respiratory capacity was observed (12). Preparation of the liver for respirometry was adapted from previous work (36). Briefly, a pair of small sections from the left lateral lobe (~6 mg each) were placed in a petri dish with ice-cold BIOPS and subjected to gentle mechanical separation with forceps under a dissecting microscope. Duplicate liver samples were blotted dry on filter paper, weighed, and placed into the respirometer chambers. To prepare skeletal muscle for respirometry, the gastrocnemius was placed in a petri dish containing ice-cold BIOPS and mechanically separated with sharp forceps into duplicate fiber bundles (~4-6 mg each) under a dissecting microscope (26, 43). Fiber bundles were then permeabilized by placing them into separate wells of a 6-well

plate filled with BIOPS containing saponin (50 µg/ml) and incubated with gentle shaking on ice for 20 minutes. Following saponin treatment, fiber bundles were washed in respiration medium (MiR05) on ice with gentle shaking for 10 min (MiR05: 0.5 mM EGTA, 3 mM $MgCl_2$, 60 mM K-lactobionate, 20 mM taurine, 10 mM KH_2PO_4, 20 mM HEPES, 110 mM Sucrose, and 1g/l BSA, pH 7.1). After washing, the fiber bundles were gently blotted dry on filter paper and weighed before being placed into the respirometer chambers.

High-resolution respirometry

In situ respiration was measured in the pre-determined order of WAT, liver, and skeletal muscle. This sequence was based on reported stability of mitochondrial performance following storage in BIOPS, with skeletal muscle showing the greatest retention of respiratory function whereas WAT shows a more rapid decline (12). Oxygen flux per tissue mass ($pmol \cdot s^{-1} \cdot mg^{-1}$) was recorded in real-time at 37°C in the oxygen concentration range of 550-350 nmol/ml using high-resolution respirometry (Oxygraph-2k, Oroboros Instruments, Innsbruck, AT) and Datlab software (Oroboros Instruments, Innsbruck, AT). In WAT and liver, respiration was assessed by a substrate-uncoupler-inhibitor-titration (SUIT) protocol adapted from Porter et al. (47, 48) containing the following sequential injections: 1) 1 mM malate, 75 µM palmitoyl-carnitine, 5 mM pyruvate, and 10 mM glutamate, to determine non-phosphorylating LEAK respiration supported by complex I linked substrates (with fatty acids) (CI_L); 2) 5 mM ADP to achieve maximal phosphorylating respiration from electron input through complex I (CI_P); 3) 10 mM succinate to saturate complex II and achieve maximal convergent electron flux through complex I and II ($CI+II_P$); 4) 10 µM cytochrome c to assess the integrity of the outer mitochondrial membrane and hence quality of sample preparation (samples were rejected when flux increased by >15% (37)); 5) 0.5 µM carbonylcyanide m-cholorophenyl hydrazone (CCCP) to assess complex I and II linked ETS capacity (i.e. maximal capacity of the electron transfer system; $CI+II_E$); 6) 0.5 µM rotenone to inhibit complex I (CII_E); and 7) 2.5 µM Antimycin A to inhibit complex III and obtain residual oxygen consumption. We note that in our evaluation of OXPHOS supported by complex I and II linked substrates (i.e. CI_P, $CI+II_P$), a fatty acid was included in the protocol, therefore, electrons are also supplied into the respiratory chain via electron-transferring flavoprotein (43).

For mitochondrial respiration in skeletal muscle, a similar SUIT protocol was followed with slight modifications to the sequence of injections in order to determine fatty acid based respiration (14): 1) 1 mM

malate and 75 µM palmitoyl-carnitine to determine LEAK respiration supported by fatty acids (FAO_L); 2) 5 mM ADP to determine fatty acid OXPHOS capacity (FAO_P); and 3) 5 mM pyruvate and 10mM glutamate to evaluate complex I supported OXPHOS capacity (with fatty acids) (CI_P). Subsequent assessment of $CI+II_P$, outer membrane integrity, $CI+II_E$, CII_E, and residual oxygen consumption were identical to steps 3-7 of the protocol used for WAT and liver.

Data reduction and analysis

Oxygen fluxes of the different respiratory states were corrected by subtracting residual oxygen consumption following antimycin A treatment. Fluxes from each duplicate measurement were averaged for statistical analysis. To determine flux control ratios, which express respiratory control independent of mitochondrial volume-density, tissue mass-specific oxygen fluxes from the SUIT protocol were divided by maximal electron transfer system capacity ($CI+II_E$) as the reference state (43). Because $CI+II_E$ is an intrinsic indicator of mitochondrial function that represents the maximal capacity of the electron transfer system, it can be used to normalize the other respiratory states (43). The respiratory control ratio (RCR), an index of coupling efficiency of the OXPHOS system, was calculated for WAT and liver in the complex I linked substrate state from the ratio of CI_P to CI_L *(P/L)* (11). The inverse RCR in the complex I supported state (*L/P*) was also calculated. To determine the fraction of maximal OXPHOS capacity serving LEAK respiration, the oxygen flux measured with complex I substrates but not adenylates, CI_L, was divided by $CI+II_P$. (11, 43) The substrate control ratio (SCR), which evaluates the change in oxygen flux by addition of substrate within a defined coupling state, was calculated for succinate ($SCR_{succinate}$) as $CI+II_P/CI_P$ (48).

Total homogenate and subcellular fractionation

Tissue homogenate (skeletal muscle, WAT, and liver) was prepared using a Potter-Elvehjem homogenizer containing 1 mL of ice-cold mitochondrial isolation buffer (215 mM mannitol, 75 mM sucrose, 0.1% BSA, 20 mM HEPES, 1 mM EGTA, and pH adjusted to 7.2 with KOH), as previously described (56). 400 µl of tissue homogenate was frozen immediately in -80 °C for biochemical assays. To isolate the mitochondria, the remaining tissue homogenate was centrifuged at 1,300 g for 3 min at 4 °C to obtain nuclear pellets. The supernatant was further centrifuged at 10,000 g for 10 min at 4 °C to obtain mitochondrial pellets.

The final mitochondrial pellet was resuspended in 40 µl isolation buffer. The protein concentration of total homogenate and mitochondrial fraction was measured using the BCA protein assay kit.

H_2O_2 production

Liver and skeletal muscle mitochondrial H_2O_2 production were measured using 50 µM Amplex Red (Cat#10187-606, BioVision) and 1 U/ml *horseradish peroxidase* (HRP) reagents at 30 °C as described previously (57). The formation of fluorescent resorufin from Amplex red was measured after a 10 min period at 530-nm excitation and 590-nm emission filters using a Biotek Synergy HTX spectrofluorometer (Winooski, VT).

Citrate synthase activity

Citrate synthase (CS) was analyzed as a surrogate for mitochondrial volume-density in homogenized liver and gastrocnemius tissues. CS activity was not assayed in WAT due to limited tissue availability. CS activity was determined using a commercially available kit according to the manufacturer's instructions (MitoCheck® Citrate Synthase Activity Assay Kit, Cayman Chemical). Absorbance was measured spectrophotometrically in 30 second intervals for 20 minutes at 412 nm. Samples were analyzed in duplicate at a tissue concentration of 2 mg/ml. CS activity was expressed as nM/min/µg protein.

Cardiolipin content

The fluorescent dye 10-N-Nonyl-Acridine Orange (Cat # A7847, Sigma) was used to measure mitochondrial cardiolipin content (24, 25). Briefly, 50 µg of liver mitochondria and white adipocyte total protein homogenate was incubated with 50 µM of NAO reagent in mitochondrial isolation buffer at 30°C for 20 min in the dark. After incubation, the red fluorescence of NAO bound to cardiolipin was measured at wavelengths of 495 nm (excitation) and 519 nm (emission) with a Biotek spectrofluorometer.

Myofiber cross-sectional area

Procedures for determining myofiber cross-sectional area (CSA) were performed as previously described (33). Briefly, transverse sections 8 µm thick were sectioned from the mid-belly of the gastrocnemius

on a cryostat at -20°C. Sections were subsequently fixed with 10% formalin, stained with hematoxylin, washed with PBS, and coverslipped with Immu-Mount medium. Images were acquired at 20x and analyzed by NIH-Image J software.

Western blotting

A total of 30 µg of protein from total homogenate or mitochondrial fraction of liver and skeletal muscle were resolved by SDS-PAGE using 4–20% Criterion™ TGX™ Precast gels (Cat# 5671095, Bio-Rad, Hercules, CA). The proteins were transferred onto polyvinylidene difluoride (PVDF) membranes, blocked with 6% nonfat dry milk or 5% BSA (for phospho-specific antibodies) for one hour at room temperature, and then incubated at 4°C overnight with the primary antibody of interest. The primary antibodies included: mitochondrial anti-adenine nucleotide translocase 2 rabbit mAb (Ant2, 1:2500 dilution, cat#14671), mitochondrial anti-uncoupling protein 2 rabbit mAb (Ucp2, 1:2500 dilution, cat#89326), anti-phospho-AMP activated protein kinase α rabbit mAb (Thr172) (p-AMPKα, 1:2000, cat#2535), total anti-AMP activated protein kinase α rabbit polyAb (AMPKα, 1:2000 dilution, cat#2532), anti-α-tubulin mouse mAb (1:5000, cat#3873) and mitochondrial anti-voltage dependent anion channel rabbit mAb (VDAC, 1:5000 dilution, cat#4661) from Cell Signaling Technology Inc. The mitochondrial anti-creatine kinase 2 rabbit polyAb (CKMT2, 1:3000 dilution, cat#SAB2100437) was from Sigma-Aldrich. For secondary antibodies, peroxidase-conjugated horse anti-mouse IgG (cat#7076) and goat anti-rabbit IgG (cat # 7074) were obtained from Cell Signaling Technology. The immunoreactive protein reaction was revealed using SuperSignal™ West Pico PLUS Chemiluminescent Substrate (cat# PI34580, Thermo Fisher). The reactive bands were detected by ChemiDoc™ XRS+ imaging system (Bio-rad) and density measured using NIH ImageJ software.

Statistical analysis

All data are reported as mean±SE. Group differences were determined by one-way ANOVA. In the event of a significant F-test, *post hoc* analysis was conducted using Tukey's HSD. Pearson correlation coefficients (r) were used to determine the associations among mitochondrial respiration, percent body weight change, myofiber cross-sectional area and protein expression. To obtain the proportion of shared variance

between these variables, the coefficient of determination (R^2) was calculated for each correlation by squaring the Pearson-r value. Significance was accepted at $p<0.05$.

Results

Weight loss and organ atrophy in colon-26 tumor-induced cachexia

Body weight change averaged -10±1% in C26-MOD, and -22±2 % in C26-SEV, which were significantly different from PBS-WS and C26-WS (Fig. 1a). Weight loss was also significantly greater in C26-SEV compared to C26-MOD (Fig. 1a). Tumor burden increased in accordance with weight loss (Fig. 1b). Muscle weights were ~20-30% lower in C26-MOD and C26-SEV compared to PBS-WS and C26-WS (Fig. 1c). Epididymal fat was substantially depleted in C26-MOD relative to PBS-WS and C26-WS; epididymal fat was not detected in C26-SEV. (Fig. 1d). The spleen was significantly enlarged in C26-WS and C26-MOD versus PBS-WS (+44-74%) (Fig. 1e), consistent with an inflammatory response to tumor load. Although spleen mass was 34% greater in C26-SEV compared to PBS-WS, this did not reach statistical significance ($p=0.183$). Absolute liver mass was lower in C26-MOD and C26-SEV compared to the WS groups (Fig. 1f). Fiber cross-sectional area was ~45% lower in C26-MOD, and ~55% lower in C26-SEV compared to the WS groups (Fig. 1g-h). Fiber size distribution revealed the greatest percentage of small fibers in C26-SEV, followed by C26-MOD (Fig. 1i).

Impairment of complex I-supported skeletal muscle mitochondrial respiration in severe cachexia

In comparison to PBS-WS and C26-WS, mass-specific fluxes for FAO_L, FAO_P, CI_P, $CI+II_P$, and $CI+II_E$ were lower in C26-MOD and C26-SEV (Fig. 2a), indicating a general cachexia-associated loss of muscle respiratory capacity per tissue mass under various substrate and coupling states. In particular, CI_P, $CI+II_P$, and $CI+II_E$ were 23-40% lower in C26-MOD, and 58-79% lower in C26-SEV (Fig. 2a). Oxygen flux for select substrate and coupling states were also lower in C26-SEV compared to C26-MOD (Fig. 2a), supportive of a progressive deterioration in muscle mitochondrial function per tissue mass as cachexia severity increased. There were no differences in CS activity ($p>0.05$) (Fig. 2d), consistent with an impairment of skeletal muscle respiration in cachexia as opposed to a reduced mitochondrial volume-density. Mass-specific fluxes FAO_L,

306 FAO_P, CI_P, $CI+II_P$, and $CI+II_E$ each related linearly with body weight change (r=0.689-0.804) and fiber CSA
307 (r=0.684-0.762) (Figs. S1a-e, h-l, doi.org/10.6084/m9.figshare.7880999.v2).
308 Normalization of mass-specific fluxes to ETS capacity, an internal mitochondrial marker, yielded flux
309 control ratios that are independent of mitochondrial density, therefore providing an index of mitochondrial
310 quality. The flux control ratio for FAO_P ($FAO_P/CI+II_E$) was 33% lower in C26-MOD (p=0.058), and 60% lower in
311 C26-SEV (p=0.001) compared to PBS-WS (data not shown). $FAO_P/CI+II_E$ in C26-SEV was also lower than
312 C26-WS (-51%, p=0.007) and C26-MOD (-40%, p=0.086) (data not shown). Suppression of fatty acid based
313 respiration may therefore depend on cachexia severity. The flux control ratio for CI_P ($CI_P/CI+II_E$) was 44-53%
314 lower in C26-SEV compared to PBS-WS, C26-WS, and C26-MOD (Fig. 2b). The lower ETS-normalized CI_P in
315 C26-SEV suggests that muscle mitochondrial quality was impaired, primarily as a consequence of severe, late
316 stage cachexia, and that the source of this dysfunction may reside at complex I. The substrate control ratio for
317 succinate, $SCR_{succinate}$, was ~4-5-fold greater in C26-SEV compared to PBS-WS, C26-WS, and C26-MOD (Fig.
318 2c). This may implicate a compensatory reliance of severely cachectic muscle on electron supply through
319 complex II in order to stimulate OXPHOS. Body weight change related significantly with both $CI_P/CI+II_E$
320 (r=0.487) and $SCR_{succinate}$ (r=-0.476) (Fig. S1f-g, doi.org/10.6084/m9.figshare.7880999.v2).
321 H_2O_2 in the mitochondrial fraction of skeletal muscle was ~40-50% lower in C26-MOD and C26-SEV
322 compared to PBS-WS and C26-WS (Fig. 2e). Phosphorylation of AMPK was ~100-150% greater in C26-WS
323 and C26-MOD compared to PBS-WS (Fig. 3a, c), indicating early activation of AMPK in skeletal muscle.
324 CKMT2 expression in C26-MOD was ~4-fold greater than PBS-WS, and ~2-fold greater than C26-WS
325 (p=0.091) and C26-SEV (p=0.054) (Fig. 3b, d), consistent with energetically stressed skeletal muscle in early
326 cachexia. Ant2 expression showed a similar pattern of response to CKMT2 (Fig. 3b, e).
327
328 *Increased respiratory rates and uncoupling in WAT during the induction of cancer cachexia*
329 Mass-specific fluxes for WAT including CI_L, CI_P, $CI+II_P$, and $CI+II_E$ were significantly greater in C26-
330 MOD compared to the WS groups (Fig. 4a), consistent with an increase in overall mitochondrial electron
331 transport and respiratory capacity. CI_L in particular showed robust expansion, exceeding the WS groups by
332 ~200% (Fig. 4a). This reflects greater leakiness of the inner mitochondrial membrane. RCR for WAT was
333 ~50% lower in C26-MOD compared to the WS groups (Fig. 4b), suggesting loss of OXPHOS coupling

efficiency. The LEAK to OXPHOS ratios *L/P* and $CI_L/CI+II_P$ were greater in C26-MOD by 85-94% and 55-86% respectively, compared to the WS groups (Figs. 4c-d). Flux control ratio for CI_L ($CI_L/CI+II_E$) was also greater in C26-MOD, by 47-75%, compared to the WS groups (Fig. 4e). These elevated LEAK ratios are consistent with uncoupled mitochondria. Cardiolipin content was ~50% lower in C26-MOD compared with C26-WS (Fig. 4f). CI_L, $CI+II_P$, and $CI+II_E$ were inversely related to body weight change (r=-0.772-0.834) and fiber CSA (r=-0.732-.817) (Figs. S2a-c, g-l, doi.org/10.6084/m9.figshare.7881110.v1), indicating elevated WAT metabolic capacity in weight-losing mice with smaller myofibers, and lower WAT metabolism in weight-stable mice with larger myofibers. Further, RCR for WAT was positively associated with body weight change and fiber CSA (r=0.709, r=0.565) (Fig. S2d, j, doi.org/10.6084/m9.figshare.7881110.v1), whereas the LEAK ratios *L/P* and $CI_L/CI+II_P$ related inversely with body weight change and fiber CSA (r=-0.628-0.789) (Fig. S2e-f, k-l, doi.org/10.6084/m9.figshare.7881110.v1), suggesting uncoupled WAT mitochondria to be a feature of tumor-induced weight loss and myofiber atrophy.

Severity dependent loss of liver OXPHOS coupling efficiency and elevated LEAK in C26 mice

Compared with PBS-WS, mass-specific respiration for CI_L, CI_P, $CI+II_P$, and $CI+II_E$ were ~40-80% lower in all three C26 groups, indicating loss of liver respiratory capacity due to cancer, and not cachexia per se, for each coupling state (i.e. LEAK, OXPHOS, ETS) (Fig. 5a). CS activity, a proxy for mitochondrial volume-density, was not different between groups ($p>0.05$) (Fig. 5e), suggesting the impairment of liver respiratory function to be independent of mitochondrial mass. AMPK phosphorylation status, an upstream signal for PGC-1α-dependent mitochondrial biogenesis, was not different between groups ($p>0.05$) (e.g. see Fig. 6b, e). RCR of the liver was ~25-60% lower in C26-WS, C26-MOD, and C26-SEV compared to PBS-WS (Fig. 5b). C26-SEV also had lower liver RCR than C26-MOD (Fig. 5b). Together this may signify a severity dependent loss of OXPHOS coupling efficiency due to cancer, which subsequently worsens when severe cachexia develops.

$CI_L/CI+II_P$ was greater in C26-WS (+82%), C26-MOD (+74%), and C26-SEV (+93%) compared to PBS-WS (Fig. 5c), consistent with an early, sustained increase in the fraction of maximal OXPHOS capacity that is LEAK due to cancer rather than cachexia. The *P/E* ratio ($CI+II_P/CI+II_E$) was greater in C26-SEV compared to all other groups (Fig. 5d). Because *P/E* in C26-SEV approached 1.0 (0.94±0.05), this may indicate dyscoupled liver mitochondria in severe cancer cachexia.

Mass-specific respiration was positively related to body weight change (r=0.382-0.430) and fiber CSA (r=0.395-0.459) (Figs. S3a-c, g-j, doi.org/10.6084/m9.figshare.7881143.v1), suggesting that depression in liver mitochondrial function may be linked to cachexia-related weight loss and fiber atrophy. Liver RCR (r=0.497) was positively associated with weight change. Thus, LEAK ratios *L/P* (r=-0.569) and $CI_L/CI+II_E$ (r=-0.484) were inversely related to weight change (Figs. S3d-f, doi.org/10.6084/m9.figshare.7881143.v1). This suggests that liver mitochondria with tighter coupling appeared more often in weight-stable mice, whereas uncoupling typically appeared with weight loss.

Decreased ROS, increased cardiolipin, and greater Ant2 expression in cachectic liver mitochondria

To identify events associated with uncoupling of OXPHOS and elevated LEAK, we measured H_2O_2 production and cardiolipin content by amplex red and NAO fluorescence, respectively, in the mitochondrial fraction of the liver. H_2O_2 is an indicator of mitochondrial ROS emission, and uncoupling may occur as a protective response against high levels of ROS. H_2O_2 declined in a severity-dependent manner compared to PBS-WS (Fig. 5f). This gradual decline in ROS emission paralleled the decrease in respiratory capacity, and may represent part of a broad, cachexia-associated loss of liver mitochondrial function. Cardiolipin, a phospholipid of the mitochondrial inner membrane that regulates OXPHOS function, was ~40% greater in C26-MOD and C26-SEV compared to C26-WS (Fig. 5g). The greater cardiolipin content in both groups of cachectic mice may support an involvement of this mitochondrial phospholipid in the uncoupling of liver OXPHOS in cancer cachexia. We next probed for Ucp2 and Ant2 expression in liver mitochondria by immunoblotting to determine whether proteins with reported uncoupling properties may be associated with the increased LEAK respiration and uncoupling of OXPHOS (Fig. 6a). Ucp2 protein expression was not significantly different between groups ($p>0.05$) (Fig. 6a, c). However, Ant2 protein expression was significantly greater in C26-SEV compared to PBS-WS, C26-WS, and C26-MOD, by 30%, 15%, and 16%, respectively (Fig. 6a, d). There was a significant inverse relationship between Ant2 expression and RCR in the liver (r=-0.547), implying higher liver Ant2 content to be associated with uncoupling of OXPHOS (Fig. 6f).

Discussion

We report tissue-specific alterations in mitochondrial function during colon-26 tumor-induced cachexia. The progression and characteristics of mitochondrial function adaptations differed among skeletal muscle, liver and WAT; but there were no differences in CS activity, consistent with impaired respiratory control that was independent of changes in tissue mitochondrial volume-density. In liver, ETS and OXPHOS capacity and RCR decreased in tumor-bearing mice, even before weight loss was observed. Weight loss and muscle atrophy was linearly correlated with these effects. The impairment of liver mitochondrial respiration was associated with increased cardiolipin and Ant2 but not Ucp2 expression. These data suggest roles for Ant2 and cardiolipin in uncoupling of liver OXPHOS. In WAT, the first effects on mitochondrial respiration were observed in mice with moderate cachexia. The induction of moderate cachexia was associated with an increase in ETS and OXPHOS capacities, an increase in non-phosphorylating LEAK respiration, and a decrease in RCR, consistent with the uncoupling of respiration from ATP synthesis. Weight loss and muscle atrophy were linearly correlated with these effects. In skeletal muscle, ETS and OXPHOS capacity were reduced in severe cachexia. Adaptation in mitochondrial respiratory control in skeletal muscle resided at complex I. Overall, mitochondrial respiratory variables in liver, WAT, and skeletal muscle accounted for a significant proportion of the variance in body weight change and myofiber size (Figs. S1, S2, S3). These findings suggest that mitochondrial function is subject to tissue-specific control during cancer cachexia, whereby early alterations arise in liver and WAT, followed by later impairment of skeletal muscle respiration (Fig. 7).

Skeletal muscle is the most widely studied organ in cancer cachexia. Several pre-clinical investigations examined *in situ* mitochondrial respiration in skeletal muscle using a cross-sectional design comparing controls and tumor-bearing rodents with marked cachexia. Impaired complex I and complex II OXPHOS were reported (23, 31), consistent with a loss of mitochondrial respiratory capacity and altered respiratory control in severely cachectic skeletal muscle. We expand upon these findings by evaluating *in situ* respiration across a range of coupling states and substrate conditions, in tissue obtained from tumor-bearing mice with varying degrees of cachexia severity. In skeletal muscle, reduction in mass-specific complex I and complex I+II OXPHOS and ETS capacities only occurred in severe cachexia, suggesting that altered skeletal muscle mitochondrial respiration is not an early event in cancer cachexia. Loss of muscle mass and fiber CSA were evident in mice with moderate cachexia despite no significant impairment of complex I and II linked respiration compared with

saline control. The exception to this was that fatty acid driven respiratory capacity (i.e. FAO_L, FAO_P) was reduced in moderate cachexia and remained suppressed in the severe state.

Since these parameters represent tissue mass-specific fluxes and do not account for changes in mitochondrial volume-density, we also calculated flux control ratios by normalization to maximal ETS capacity to provide indices of mitochondrial quality that are independent of mitochondrial density. The flux control ratio for complex I OXPHOS in skeletal muscle was impaired only in severe cachexia, consistent with the notion that muscle mitochondrial dysfunction occurred only in late-stage cachexia. The substrate control ratio for succinate was ~4-5 fold greater in severe cachexia, an apparent compensation for complex I dysfunction, to stimulate OXPHOS via complex II. Impairment in OXPHOS capacity could contribute to energetic stress in skeletal muscle of cachectic mice. We found that phosphorylation of AMPK was increased early, in weight-stable C26 mice, and remained elevated in moderate cachexia. This implies that energetic stress precedes protein degradation and muscle atrophy. The ~2-4-fold increase in mitochondrial creatine kinase (CKMT2) expression in moderate cachexia is consistent with this implication; this could represent a compensatory adaptation to protect oxidative energy provision in skeletal muscle (56). A similar expression pattern was seen for Ant2, an ADP transport protein, suggesting that Ant2 may also be involved in this compensation. In addition to impaired OXPHOS, dysfunctional mitochondria may generate high levels of ROS that in turn affects protein turnover and causes atrophy. We did not observe increased H_2O_2 in the mitochondrial fraction of skeletal muscle as anticipated. H_2O_2 production actually declined in moderate and severe cachexia (perhaps consequent to reduced ETS capacity in these conditions) and does not appear associated with muscle atrophy in this model.

The elevated rates of mitochondrial respiration in WAT were not surprising. A recent report found increased oligomycin and FCCP induced respiration in white adipocytes treated with parathyroid hormone-related protein, a tumor-derived product that induces beiging (35). Others found increased respiratory capacity of beige-like WAT in cachectic mice using glycerol-3-phosphate as a substrate (44). Our data extends these findings by evaluating *in situ* respiration of WAT in a broader spectrum of coupling and substrates states. A unique finding was the increase in coupled (phosphorylating) respiration with electron input through complex I and complex I+II, which to our knowledge has not been previously reported. Upregulation of TCA cycle, electron transport, and OXPHOS genes in WAT of cancer patients with cachexia has been documented by

446 others (17), and our elevated OXPHOS and ETS capacities are consistent with that gene profile. The increase
447 in phosphorylating respiration could be a compensatory response to mitochondrial uncoupling in WAT, leading
448 to increased energy expenditure. Alternatively, increased OXPHOS and ETS capacity could be related to
449 lipolysis and intracellular accumulation of free fatty acids. Treatments that inhibit coupling and ATP synthesis
450 are believed to suppress lipogenesis in adipose tissue (9, 51). Further, insulin-dependent suppression of
451 lipolysis may depend on ATP availability (9, 54). Thus, increased phosphorylating respiration capacity may be
452 a compensatory effort to provide the energy supply to promote lipogenesis and/or suppress lipolysis, in order
453 to maintain adipose mass in the face of tumor-induced catabolism.

454 While coupled respiration of WAT increased in early cachexia, the LEAK state increased dramatically.
455 By dividing coupled and LEAK respiration (in the same complex I-linked substrate conditions), we obtained the
456 respiratory control ratio (RCR), an index of OXPHOS coupling efficiency. Because LEAK expanded to a much
457 larger degree relative to coupled respiration, WAT RCR decreased in early cachexia relative to weight-stable
458 mice. The presence of elevated LEAK was a consistent finding in this study, with greater WAT LEAK in early
459 cachexia even when normalized to maximal OXPHOS and ETS capacities. These findings are significant
460 because they imply increased resting energy expenditure. In burn injury, WAT undergoes browning and shows
461 high LEAK respiration in parallel with elevated resting energy expenditure. Reprogramming of WAT
462 metabolism in this manner could potentially contribute to hypermetabolism in cancer cachexia. Therapies that
463 normalize WAT mitochondrial function by reducing LEAK and promoting tighter OXPHOS coupling may be
464 beneficial.

465 Despite exerting major control over systemic metabolism, mitochondrial function in liver is not well
466 studied in cancer cachexia. Therefore, we measured *in situ* respiration in permeabilized liver samples. The
467 three C26 groups all showed significantly lower oxygen flux compared to PBS-injected mice, suggesting that
468 the tumor was mainly responsible for impairment of hepatic mitochondrial respiration per unit of tissue mass.
469 RCR was also lower in all three C26 groups, although C26 mice with severe cachexia had the greatest decline.
470 These data suggest that early loss of OXPHOS coupling efficiency in the liver arises from tumor load, and
471 subsequently worsens as cachexia severity increases. Consistent with this, the *P/E* ratio was greatest in mice
472 with severe cachexia. A *P/E* ratio that approaches 1, as was the case in the severely cachectic mice, implies

the presence of dyscoupled mitochondria (i.e. pathologically uncoupled) (43) that would be energetically inefficient, and increase resting energy expenditure.

We are aware of only a few prior investigations on liver mitochondrial energetics in cancer cachexia. Using rats bearing the peritoneal carcinoma as a model of cancer cachexia, Dumas et al. reported reduced P/O and increased energy wasting in liver mitochondria (20), events consistent with our finding of reduced liver RCR. They also found the increased energy wasting to be associated with greater cardiolipin content (R^2=0.64). In the present work, cardiolipin content increased in moderate cachexia, and stayed elevated in the severe state, consistent with their findings. The expansion of cardiolipin mass in liver is of note given that in the elderly, and in many pathologies (e.g. heart failure, Barth syndrome, ischemia-reperfusion injury), modifications to cardiolipin profiles typically consist of decreased content, altered fatty acid composition, and/or peroxidation (15). We are unable to address whether changes in composition occurred, however the decreased H_2O_2 in liver mitochondrial lysates during cachexia suggests minimal peroxidation due to mitochondrial ROS emission. We cannot exclude the possibility, though, of low antioxidant capacity and high oxidative stress. Treatment of normal liver mitochondria with cardiolipin-enriched liposomes has been shown to adversely affect ATP synthesis and increase non-phosphorylating respiration, offering a possible explanation for the significance of enhanced liver cardiolipin in cancer cachexia (21, 32).

The role of Ant in mediating cachexia-associated energy wasting has received some attention (32). Ant is an ADP/ATP exchanger in the inner mitochondrial membrane that has uncoupling capability. Treatment of liver mitochondria from cachectic rats with carboxyatractylate, an inhibitor of Ant, did not mitigate energy wasting, suggesting that Ant is not a major contributor to LEAK respiration in liver mitochondria from cachectic rodents. Therefore, inefficiency of OXPHOS and energy wasting may depend on cardiolipin, but not Ant. However, we observed a significant inverse relationship between Ant2 and RCR in the liver, suggesting a potential role for Ant2 expression to be involved in uncoupling. Direct manipulations of liver Ant2 are necessary to better understand the role of this molecule in OXPHOS function in cancer cachexia. We also anticipated an increase in Ucp2 expression in liver mitochondria from C26 mice with cachexia. Although Ucp2 expression was ~2-fold greater in C26 mice compared to PBS-WS, this did not reach statistical significance. Therefore, the increased LEAK respiration and uncoupling of OXPHOS does not appear to be mediated by Ucp2, at least in colon-26 tumor-induced cachexia. These findings bring attention to the previously

underappreciated role of liver mitochondrial function in cancer cachexia, and suggest a benefit of therapies that improve mitochondrial function of the liver.

We note several limitations in this investigation. Food intake measurements were incomplete and are therefore not reported. This information is needed to determine whether or not tumor-induced anorexia is present, and by extension if muscle mass changes relate in part to energy intake. A previous study using C26 cells sourced from the same bank reported no anorexia in cachexic C26 mice (4), and this could be a possible indication that our C26 mice would also not exhibit significant anorexia. However, this suggestion remains to be verified. Food intake and nutrient absorption are also important, due to the potential impact of fed versus prolonged fasted states on OXPHOS and ETS capacity (29). Furthermore, assessment of whole body metabolism was not performed, and this would have been a key addition in order to relate alterations at the mitochondrial level to the whole body. For instance, the broader physiological significance of tissue-specific changes in mitochondrial respiration could be demonstrated by their relationship to a whole body measurement such as resting energy expenditure, which is elevated in cachexia. Another important consideration is the identification of upstream triggers, such as tumor-derived products, that may be responsible for the effects we observed. Others have reported interleukin-6 and parathyroid hormone-related protein to be triggers of white adipose beiging (35, 44), and they could be possible candidates for our mitochondrial alterations in adipose. Whether inflammatory cytokines or tumor-derived products account for our observed effects in liver are uncertain. We did not analyze tumors or plasma to screen for potential triggers of mitochondrial dysregulation, and this merits further experimental consideration.

Lastly, we note that our tissue collection methods were adopted from prior investigations with modifications in order to attain 10% and 20% weight loss in moderate and severe cachexia, respectively. Body weight was routinely monitored to determine the timing of tissue collection, however, any measurement taken before sacrifice would be confounded by tumor weight. Thus, we drew upon our previous experience with this model, anticipating a final tumor mass at necropsy of ~2g with severe cachexia (20% weight loss), and tumor mass of ~1g at moderate (10% weight loss). For the typical adult Balb/c male weighing 25g, 1g tumor mass would account for ~3-4% of body weight. During routine monitoring, a mouse showing ~7% weight loss would be euthanized in anticipation of tumor mass accounting for ~3-4% of body weight, in order to attain the target weight loss of 10% for the moderate cachexia group. This deviates somewhat in comparison to other groups

that also study cachexia severity in the C26 model. For instance, Zimmers laboratory use 5%, 10%, and 15% weight loss for mild, moderate, and severe cachexia, respectively (8). When one group of mice reaches 10% weight loss (weight measurements include the tumor), all other groups are euthanized (8). This uniform timing of tissue collection differed from the present work, and this methodological difference should be considered when making comparisons between investigations.

In conclusion, we provide evidence for tissue-specific adaptation in mitochondrial respiratory control in colon-26 tumor-induced cachexia. Impairment of skeletal muscle mitochondrial OXPHOS occurred predominantly in severe, late stage cachexia, whereas negative adaptations in mitochondria of liver and WAT, including increased LEAK and reduced coupling control, were found earlier in cachexia progression and could contribute to increased whole body energy expenditure and involuntary weight loss characteristic of cancer cachexia. Together these findings suggest mitochondrial function of multiple tissues to be potential sites of targeted therapies.

Perspectives and Significance

There are currently no approved treatments for cancer cachexia, which occurs in up to 80% of advanced cancer patients and accounts for an estimated 20% of cancer-related deaths. Paths toward effective treatments are complicated in part by the systemic nature of the disease, where dysfunction of multiple organs contributes to the cachexic phenotype. Unraveling the mechanisms by which multi-organ remodeling contributes to cachexia are necessary in order to devise supportive care and treatment strategies that improve the lives of affected cancer patients. Here we contribute to the understanding of some of these mechanisms. We identify tissue-specific responses that mitochondria undergo at varying degrees of cachexia severity. We show that mitochondria in both muscle and non-muscle organs (liver, adipose) are involved in the onset of moderate cachexia, and appear to also regulate progression towards a severe presentation of the disease. Targeting mitochondrial function in a variety of tissue types, and defining how those targeted manipulations impact cachexia onset and progression, are important next steps to show which mitochondrial mechanisms could be exploited to improve patient outcomes.

Acknowledgements

We extend our sincere thanks to Dr. Chun-Jung Huang, Director of the Exercise Biochemistry Laboratory, for research support, and Joseph P. Carzoli and Trevor K. Johnson for technical assistance. JLH was supported by an Undergraduate Research Fellowship (SURF) from the Office of Undergraduate Research and Inquiry at Florida Atlantic University.

Conflict of Interest

The authors declare no conflict of interest.

References

1. **Andreux PA, Houtkooper RH, and Auwerx J**. Pharmacological approaches to restore mitochondrial function. *Nat Rev Drug Discov* 12: 465-483, 2013.
2. **Argiles JM, Busquets S, Stemmler B, and Lopez-Soriano FJ**. Cancer cachexia: understanding the molecular basis. *Nat Rev Cancer* 14: 754-762, 2014.
3. **Argiles JM, Lopez-Soriano FJ, and Busquets S**. Muscle wasting in cancer: the role of mitochondria. *Curr Opin Clin Nutr Metab Care* 18: 221-225, 2015.
4. **Assi M, Derbre F, Lefeuvre-Orfila L, and Rebillard A**. Antioxidant supplementation accelerates cachexia development by promoting tumor growth in C26 tumor-bearing mice. *Free Radic Biol Med* 91: 204-214, 2016.
5. **Baker MJ, Palmer CS, and Stojanovski D**. Mitochondrial protein quality control in health and disease. *Br J Pharmacol* 171: 1870-1889, 2014.
6. **Baker MJ, Tatsuta T, and Langer T**. Quality control of mitochondrial proteostasis. *Cold Spring Harb Perspect Biol* 3: 2011.
7. **Bonetto A, Aydogdu T, Kunzevitzky N, Guttridge DC, Khuri S, Koniaris LG, and Zimmers TA**. STAT3 activation in skeletal muscle links muscle wasting and the acute phase response in cancer cachexia. *PloS one* 6: e22538, 2011.
8. **Bonetto A, Rupert JE, Barreto R, and Zimmers TA**. The Colon-26 Carcinoma Tumor-bearing Mouse as a Model for the Study of Cancer Cachexia. *J Vis Exp* 2016.
9. **Boudina S, and Graham TE**. Mitochondrial function/dysfunction in white adipose tissue. *Exp Physiol* 99: 1168-1178, 2014.
10. **Brown JL, Rosa-Caldwell ME, Lee DE, Blackwell TA, Brown LA, Perry RA, Haynie WS, Hardee JP, Carson JA, Wiggs MP, Washington TA, and Greene NP**. Mitochondrial degeneration precedes the development of muscle atrophy in progression of cancer cachexia in tumour-bearing mice. *J Cachexia Sarcopenia Muscle* 8: 926-938, 2017.
11. **Burtscher J, Zangrandi L, Schwarzer C, and Gnaiger E**. Differences in mitochondrial function in homogenated samples from healthy and epileptic specific brain tissues revealed by high-resolution respirometry. *Mitochondrion* 25: 104-112, 2015.
12. **Canto C, and Garcia-Roves PM**. High-Resolution Respirometry for Mitochondrial Characterization of Ex Vivo Mouse Tissues. *Curr Protoc Mouse Biol* 5: 135-153, 2015.
13. **Carson JA, Hardee JP, and VanderVeen BN**. The emerging role of skeletal muscle oxidative metabolism as a biological target and cellular regulator of cancer-induced muscle wasting. *Semin Cell Dev Biol* 54: 53-67, 2016.
14. **Chicco AJ, Le CH, Schlater A, Nguyen A, Kaye S, Beals JW, Scalzo RL, Bell C, Gnaiger E, Costa DP, Crocker DE, and Kanatous SB**. High fatty acid oxidation capacity and phosphorylation control despite elevated leak and reduced respiratory capacity in northern elephant seal muscle mitochondria. *J Exp Biol* 217: 2947-2955, 2014.
15. **Chicco AJ, and Sparagna GC**. Role of cardiolipin alterations in mitochondrial dysfunction and disease. *Am J Physiol Cell Physiol* 292: C33-44, 2007.
16. **Constantinou C, Fontes de Oliveira CC, Mintzopoulos D, Busquets S, He J, Kesarwani M, Mindrinos M, Rahme LG, Argiles JM, and Tzika AA**. Nuclear magnetic resonance in conjunction with functional genomics suggests mitochondrial dysfunction in a murine model of cancer cachexia. *International journal of molecular medicine* 27: 15-24, 2011.
17. **Dahlman I, Mejhert N, Linder K, Agustsson T, Mutch DM, Kulyte A, Isaksson B, Permert J, Petrovic N, Nedergaard J, Sjolin E, Brodin D, Clement K, Dahlman-Wright K, Ryden M, and Arner P**. Adipose tissue pathways involved in weight loss of cancer cachexia. *Br J Cancer* 102: 1541-1548, 2010.
18. **Di Marco S, Cammas A, Lian XJ, Kovacs EN, Ma JF, Hall DT, Mazroui R, Richardson J, Pelletier J, and Gallouzi IE**. The translation inhibitor pateamine A prevents cachexia-induced muscle wasting in mice. *Nat Commun* 3: 896, 2012.
19. **Diffee GM, Kalfas K, Al-Majid S, and McCarthy DO**. Altered expression of skeletal muscle myosin isoforms in cancer cachexia. *Am J Physiol Cell Physiol* 283: C1376-1382, 2002.
20. **Dumas JF, Goupille C, Julienne CM, Pinault M, Chevalier S, Bougnoux P, Servais S, and Couet C**. Efficiency of oxidative phosphorylation in liver mitochondria is decreased in a rat model of peritoneal carcinosis. *J Hepatol* 54: 320-327, 2011.
21. **Dumas JF, Peyta L, Couet C, and Servais S**. Implication of liver cardiolipins in mitochondrial energy metabolism disorder in cancer cachexia. *Biochimie* 95: 27-32, 2013.

22. **Fearon K, Arends J, and Baracos V**. Understanding the mechanisms and treatment options in cancer cachexia. *Nat Rev Clin Oncol* 10: 90-99, 2013.
23. **Fermoselle C, Garcia-Arumi E, Puig-Vilanova E, Andreu AL, Urtreger AJ, de Kier Joffe ED, Tejedor A, Puente-Maestu L, and Barreiro E**. Mitochondrial dysfunction and therapeutic approaches in respiratory and limb muscles of cancer cachectic mice. *Exp Physiol* 98: 1349-1365, 2013.
24. **Gallet PF, Maftah A, Petit JM, Denis-Gay M, and Julien R**. Direct cardiolipin assay in yeast using the red fluorescence emission of 10-N-nonyl acridine orange. *Eur J Biochem* 228: 113-119, 1995.
25. **Garcia Fernandez MI, Ceccarelli D, and Muscatello U**. Use of the fluorescent dye 10-N-nonyl acridine orange in quantitative and location assays of cardiolipin: a study on different experimental models. *Anal Biochem* 328: 174-180, 2004.
26. **Gnaiger E**. Capacity of oxidative phosphorylation in human skeletal muscle: new perspectives of mitochondrial physiology. *Int J Biochem Cell Biol* 41: 1837-1845, 2009.
27. **Goncalves MD, Hwang SK, Pauli C, Murphy CJ, Cheng Z, Hopkins BD, Wu D, Loughran RM, Emerling BM, Zhang G, Fearon DT, and Cantley LC**. Fenofibrate prevents skeletal muscle loss in mice with lung cancer. *Proc Natl Acad Sci U S A* 115: E743-E752, 2018.
28. **Heim AB, Chung D, Florant GL, and Chicco AJ**. Tissue-specific seasonal changes in mitochondrial function of a mammalian hibernator. *Am J Physiol Regul Integr Comp Physiol* 313: R180-R190, 2017.
29. **Hoeks J, van Herpen NA, Mensink M, Moonen-Kornips E, van Beurden D, Hesselink MK, and Schrauwen P**. Prolonged fasting identifies skeletal muscle mitochondrial dysfunction as consequence rather than cause of human insulin resistance. *Diabetes* 59: 2117-2125, 2010.
30. **Inagaki J, Rodriguez V, and Bodey GP**. Proceedings: Causes of death in cancer patients. *Cancer* 33: 568-573, 1974.
31. **Julienne CM, Dumas JF, Goupille C, Pinault M, Berri C, Collin A, Tesseraud S, Couet C, and Servais S**. Cancer cachexia is associated with a decrease in skeletal muscle mitochondrial oxidative capacities without alteration of ATP production efficiency. *J Cachexia Sarcopenia Muscle* 3: 265-275, 2012.
32. **Julienne CM, Tardieu M, Chevalier S, Pinault M, Bougnoux P, Labarthe F, Couet C, Servais S, and Dumas JF**. Cardiolipin content is involved in liver mitochondrial energy wasting associated with cancer-induced cachexia without the involvement of adenine nucleotide translocase. *Biochim Biophys Acta* 1842: 726-733, 2014.
33. **Khamoui AV, Park BS, Kim DH, Yeh MC, Oh SL, Elam ML, Jo E, Arjmandi BH, Salazar G, Grant SC, Contreras RJ, Lee WJ, and Kim JS**. Aerobic and resistance training dependent skeletal muscle plasticity in the colon-26 murine model of cancer cachexia. *Metabolism* 65: 685-698, 2016.
34. **Kir S, Komaba H, Garcia AP, Economopoulos KP, Liu W, Lanske B, Hodin RA, and Spiegelman BM**. PTH/PTHrP Receptor Mediates Cachexia in Models of Kidney Failure and Cancer. *Cell Metab* 23: 315-323, 2016.
35. **Kir S, White JP, Kleiner S, Kazak L, Cohen P, Baracos VE, and Spiegelman BM**. Tumour-derived PTH-related protein triggers adipose tissue browning and cancer cachexia. *Nature* 513: 100-104, 2014.
36. **Kuznetsov AV, Strobl D, Ruttmann E, Konigsrainer A, Margreiter R, and Gnaiger E**. Evaluation of mitochondrial respiratory function in small biopsies of liver. *Anal Biochem* 305: 186-194, 2002.
37. **Kuznetsov AV, Veksler V, Gellerich FN, Saks V, Margreiter R, and Kunz WS**. Analysis of mitochondrial function in situ in permeabilized muscle fibers, tissues and cells. *Nat Protoc* 3: 965-976, 2008.
38. **Lantier L, Williams AS, Williams IM, Yang KK, Bracy DP, Goelzer M, James FD, Gius D, and Wasserman DH**. SIRT3 Is Crucial for Maintaining Skeletal Muscle Insulin Action and Protects Against Severe Insulin Resistance in High-Fat-Fed Mice. *Diabetes* 64: 3081-3092, 2015.
39. **McLean JB, Moylan JS, and Andrade FH**. Mitochondria dysfunction in lung cancer-induced muscle wasting in C2C12 myotubes. *Front Physiol* 5: 503, 2014.
40. **Mishra P, and Chan DC**. Metabolic regulation of mitochondrial dynamics. *J Cell Biol* 212: 379-387, 2016.
41. **Morrow RM, Picard M, Derbeneva O, Leipzig J, McManus MJ, Gouspillou G, Barbat-Artigas S, Dos Santos C, Hepple RT, Murdock DG, and Wallace DC**. Mitochondrial energy deficiency leads to hyperproliferation of skeletal muscle mitochondria and enhanced insulin sensitivity. *Proc Natl Acad Sci U S A* 114: 2705-2710, 2017.
42. **Murphy KT, Chee A, Trieu J, Naim T, and Lynch GS**. Importance of functional and metabolic impairments in the characterization of the C-26 murine model of cancer cachexia. *Disease models & mechanisms* 5: 533-545, 2012.
43. **Pesta D, and Gnaiger E**. High-resolution respirometry: OXPHOS protocols for human cells and permeabilized fibers from small biopsies of human muscle. *Methods Mol Biol* 810: 25-58, 2012.

44. **Petruzzelli M, Schweiger M, Schreiber R, Campos-Olivas R, Tsoli M, Allen J, Swarbrick M, Rose-John S, Rincon M, Robertson G, Zechner R, and Wagner EF**. A switch from white to brown fat increases energy expenditure in cancer-associated cachexia. *Cell Metab* 20: 433-447, 2014.
45. **Petruzzelli M, and Wagner EF**. Mechanisms of metabolic dysfunction in cancer-associated cachexia. *Genes Dev* 30: 489-501, 2016.
46. **Porporato PE**. Understanding cachexia as a cancer metabolism syndrome. *Oncogenesis* 5: e200, 2016.
47. **Porter C, Herndon DN, Chondronikola M, Chao T, Annamalai P, Bhattarai N, Saraf MK, Capek KD, Reidy PT, Daquinag AC, Kolonin MG, Rasmussen BB, Borsheim E, Toliver-Kinsky T, and Sidossis LS**. Human and Mouse Brown Adipose Tissue Mitochondria Have Comparable UCP1 Function. *Cell Metab* 24: 246-255, 2016.
48. **Porter C, Hurren NM, Cotter MV, Bhattarai N, Reidy PT, Dillon EL, Durham WJ, Tuvdendorj D, Sheffield-Moore M, Volpi E, Sidossis LS, Rasmussen BB, and Borsheim E**. Mitochondrial respiratory capacity and coupling control decline with age in human skeletal muscle. *Am J Physiol Endocrinol Metab* 309: E224-232, 2015.
49. **Rana A, Oliveira MP, Khamoui AV, Aparicio R, Rera M, Rossiter HB, and Walker DW**. Promoting Drp1-mediated mitochondrial fission in midlife prolongs healthy lifespan of Drosophila melanogaster. *Nat Commun* 8: 448, 2017.
50. **Reid J, McKenna HP, Fitzsimons D, and McCance TV**. An exploration of the experience of cancer cachexia: what patients and their families want from healthcare professionals. *European journal of cancer care* 19: 682-689, 2010.
51. **Rognstad R, and Katz J**. The effect of 2,4-dinitrophenol on adipose-tissue metabolism. *Biochem J* 111: 431-444, 1969.
52. **Romanello V, and Sandri M**. Mitochondrial Quality Control and Muscle Mass Maintenance. *Front Physiol* 6: 422, 2015.
53. **Sidossis LS, Porter C, Saraf MK, Borsheim E, Radhakrishnan RS, Chao T, Ali A, Chondronikola M, Mlcak R, Finnerty CC, Hawkins HK, Toliver-Kinsky T, and Herndon DN**. Browning of Subcutaneous White Adipose Tissue in Humans after Severe Adrenergic Stress. *Cell Metab* 22: 219-227, 2015.
54. **Steinfelder HJ, and Joost HG**. Reversible reduction of insulin receptor affinity by ATP depletion in rat adipocytes. *Biochem J* 214: 203-207, 1983.
55. **Tzika AA, Fontes-Oliveira CC, Shestov AA, Constantinou C, Psychogios N, Righi V, Mintzopoulos D, Busquets S, Lopez-Soriano FJ, Milot S, Lepine F, Mindrinos MN, Rahme LG, and Argiles JM**. Skeletal muscle mitochondrial uncoupling in a murine cancer cachexia model. *Int J Oncol* 43: 886-894, 2013.
56. **Visavadiya NP, Keasey MP, Razskazovskiy V, Banerjee K, Jia C, Lovins C, Wright GL, and Hagg T**. Integrin-FAK signaling rapidly and potently promotes mitochondrial function through STAT3. *Cell Commun Signal* 14: 32, 2016.
57. **Visavadiya NP, McEwen ML, Pandya JD, Sullivan PG, Gwag BJ, and Springer JE**. Antioxidant properties of Neu2000 on mitochondrial free radicals and oxidative damage. *Toxicol In Vitro* 27: 788-797, 2013.
58. **von Haehling S, and Anker SD**. Cachexia as a major underestimated and unmet medical need: facts and numbers. *J Cachexia Sarcopenia Muscle* 1: 1-5, 2010.
59. **White JP, Baynes JW, Welle SL, Kostek MC, Matesic LE, Sato S, and Carson JA**. The regulation of skeletal muscle protein turnover during the progression of cancer cachexia in the Apc(Min/+) mouse. *PloS one* 6: e24650, 2011.
60. **Xu H, Crawford D, Hutchinson KR, Youtz DJ, Lucchesi PA, Velten M, McCarthy DO, and Wold LE**. Myocardial dysfunction in an animal model of cancer cachexia. *Life sciences* 88: 406-410, 2011.
61. **Zhou X, Wang JL, Lu J, Song Y, Kwak KS, Jiao Q, Rosenfeld R, Chen Q, Boone T, Simonet WS, Lacey DL, Goldberg AL, and Han HQ**. Reversal of cancer cachexia and muscle wasting by ActRIIB antagonism leads to prolonged survival. *Cell* 142: 531-543, 2010.

Figure Legends

Figure 1. Weight loss and organ atrophy in colon-26 tumor-induced cachexia

(a) Body weight changes of PBS Weight-Stable (n=4), C26 Weight-Stable (n=6), C26 Moderate (n=7), and C26 Severe (n=6). (b) Tumor weights of experimental groups. (c) Skeletal muscle wet weights of plantaris (PLT), gastrocnemius (GAS), and quadriceps (QUAD). (d) Epididymal white adipose tissue (WAT) wet weight. WAT was not detected (ND) in C26 severe group. (e-f) Wet weight of spleen (e) and liver (f). (g) Representative myofiber cross-sections of gastrocnemius muscle imaged at 20x. Imaged cross-sections were analyzed for all mice excluding n=1 from C26 Weight-Stable, and n=2 from C26 Severe due to unavailable tissue mounts (total analyzed n=20). (h) Mean myofiber cross-sectional area. (i) Fiber size distribution between groups displayed as relative frequency (percentage). Data presented as mean ± SE. Differences determined by one-way ANOVA. $p<0.05$ (*), $p<0.01$ (**), $p<0.001$ (***).

Figure 2. Impairment of complex I-linked skeletal muscle mitochondrial respiration in severe cachexia.

(a) Mass-specific oxygen (O_2) flux of gastrocnemius muscle determined *in situ* by a substrate-uncoupler-inhibitor titration protocol, including fatty acid supported LEAK (FAO_L) through addition of malate and palmitoyl-carnitine (M+PC); fatty acid supported oxidative phosphorylation (OXPHOS) (FAO_P) by addition of adenosine diphosphate (ADP); complex I supported OXPHOS (CI_P) by addition of pyruvate and glutamate (P+G); complex I+II supported OXPHOS ($CI+II_P$) by addition of succinate (S); maximal electron transfer system (ETS) capacity ($CI+II_E$) by stepwise addition of carbonyl cyanide m-chlorophenyl hydrazine (CCCP); and complex II ETS (CII_E) by addition of rotenone (Rot). (b) Flux control ratio for complex I supported OXPHOS ($CI_P/CI+II_E$). (c) Substrate control ratio (SCR) for succinate calculated by dividing $CI+II_P$ by CI_P. (d) Citrate synthase enzyme activity in gastrocnemius muscle homogenate. (e) Hydrogen peroxide (H_2O_2) production in quadriceps muscle mitochondria. Data presented as mean ± SE. Tissues assayed from PBS Weight-Stable (n=4), C26 Weight-Stable (n=6), C26 Moderate (n=7), and C26 Severe (n=6). Differences determined by one-way ANOVA. $p<0.05$ (*), $p<0.01$ (**), $p<0.001$ (***).

Figure 3. AMPK activation and ADP transport proteins in skeletal muscle of colon-26 mice.

(a-b) Immunoblots for p-AMPKα, AMPKα, mitochondrial creatine kinase (CKMT2), Ant2, and tubulin in skeletal muscle homogenate. (c) p-AMPKα expression normalized to total AMPKα. (d) CKMT2 normalized to tubulin. (e) Ant2 normalized to tubulin. Data presented as mean ± SE. Tissues assayed from PBS Weight-Stable (n=4), C26 Weight-Stable (n=6), and C26 Moderate (n=7). Differences determined by one-way ANOVA. $p<0.05$ (*), $p<0.01$ (**).

Figure 4. Increased respiratory rates and uncoupling in white adipose tissue (WAT).

(a) Mass-specific oxygen (O_2) flux of WAT determined *in situ* by a substrate-uncoupler-inhibitor titration protocol, including complex I supported LEAK (CI_L) through addition of malate (M), pyruvate (P), palmitoyl-carnitine (PC), and glutamate (G); complex I supported oxidative phosphorylation (OXPHOS) (CI_P) by addition of adenosine diphosphate (ADP); complex I+II supported OXPHOS ($CI+II_P$) by addition of succinate (S); maximal electron transfer system (ETS) capacity ($CI+II_E$) by stepwise addition of carbonyl cyanide m-chlorophenyl hydrazine (CCCP); and complex II ETS (CII_E) by addition of rotenone (Rot). (b) Respiratory control ratio (RCR) determined by dividing CI_P by CI_L. (c) *L/P* determined by dividing CI_L by CI_P. (d) Ratio of CI_L and maximal OXPHOS ($CI+II_P$). (e) Ratio of CI_L and maximal ETS capacity ($CI+II_E$). (f) Cardiolipin content in WAT homogenate. Data presented as mean ± SE. Tissues assayed from PBS Weight-Stable (n=4), C26 Weight-Stable (n=6), and C26 Moderate (n=7). Epididymal WAT was not detected in C26 Severe and thus unavailable for analysis. Differences determined by one-way ANOVA. $p<0.05$ (*), $p<0.01$ (**), $p<0.001$ (***).

Figure 5. Early loss of liver respiratory function and coupling efficiency in colon-26 mice.

(a) Mass-specific oxygen (O_2) flux of liver measured *in situ* by a substrate-uncoupler-inhibitor titration protocol, including complex I supported LEAK (CI_L) through addition of malate (M), pyruvate (P), palmitoyl-carnitine (PC), and glutamate (G); complex I supported oxidative phosphorylation (OXPHOS) (CI_P) by addition of adenosine diphosphate (ADP); complex I+II supported OXPHOS ($CI+II_P$) by addition of succinate (S); maximal electron transfer system (ETS) capacity ($CI+II_E$) by stepwise addition of carbonyl cyanide m-chlorophenyl hydrazine (CCCP); and complex II ETS (CII_E) by addition of rotenone (Rot). (b) Respiratory control ratio (RCR), calculated by dividing CI_P by CI_L. (c) Ratio between CI_L and maximal OXPHOS ($CI+II_P$). (d) The *P/E*

ratio, calculated as maximal OXPHOS (CI+II$_P$) divided by maximal ETS capacity (CI+II$_E$). (e) Citrate synthase enzyme activity in liver homogenate. (f) Hydrogen peroxide (H_2O_2) production in liver mitochondria. (g) Cardiolipin content in liver mitochondria. Data presented as mean ± SE. Tissues assayed from PBS Weight-Stable (n=4), C26 Weight-Stable (n=6), C26 Moderate (n=7), and C26 Severe (n=6). Differences determined by one-way ANOVA. $p<0.05$ (*), $p<0.01$ (**), $p<0.001$ (***).

Figure 6. Elevated expression of Ant2 but not Ucp2 in cachectic liver mitochondria of colon-26 mice. (a) Immunoblots for Ucp2, Ant2, and VDAC in mitochondrial lysates from the liver. (b) Immunoblots for p-AMPK, AMPK, and tubulin in liver homogenate. (c) Ucp2 expression normalized to VDAC. (d) Ant2 expression normalized to VDAC. (e) p-AMPK normalized to total AMPK. (f) Association of Ant2 expression with respiratory control ratio (RCR) in the liver. Data presented as mean ± SE. Tissues assayed from PBS Weight-Stable (n=4), C26 Weight-Stable (n=6), C26 Moderate (n=7), and C26 Severe (n=6). Differences determined by one-way ANOVA. $p<0.05$ (*), $p<0.01$ (**).

Figure 7. Proposed mechanisms linking tissue-specific mitochondrial function to cancer cachexia. During the induction of moderate cachexia, mitochondrial respiration is impacted in white adipose tissue and liver, but not skeletal muscle. White adipose mitochondria show drastically elevated LEAK respiration, a surrogate of proton leak. The drastic expansion of LEAK lowers the respiratory control ratio (RCR), an index of oxidative phosphorylation (OXPHOS) coupling efficiency. Thus, white adipose mitochondria are uncoupled, and this may increase resting energy expenditure (REE) and cause involuntary weight loss. In severe cachexia, white adipose becomes depleted and measurements of respiration are not available (N/A). In the cachexic liver, mitochondria are also uncoupled, due to reduced OXPHOS and increased LEAK. Cardiolipin content is increased, which contributes to LEAK and uncoupling. The persistent elevation of cardiolipin across cachexia severity suggests a role for this inner membrane phospholipid in the maintenance of the cachexic state. Adenine nucleotide translocase 2 (Ant2) also contributes to uncoupling in the liver, and is only increased in severe cachexia, suggesting that the transition to severe disease may depend on hepatic Ant2. Cachexic liver mitochondria, therefore, are uncoupled and energetically inefficient, which may increase energy expenditure and cause unintended weight loss. In skeletal muscle, impairment of OXPHOS occurs primarily in

severe cachexia due to dysfunction at complex I (CI). Attempted compensation occurs by electron supply into complex II, as reflected by the increased substrate control ratio (SCR) for succinate. Restricted ATP provision from impaired OXPHOS in skeletal muscle may contribute to atrophy, exercise intolerance and fatigue in cachexic cancer patients, thereby reducing quality of life. AMPK, adenosine monophosphate-activated protein kinase. CKMT2, mitochondrial creatine kinase 2.

Figure S1.

doi.org/10.6084/m9.figshare.7880999.v2

Figure S2.

doi.org/10.6084/m9.figshare.7881110.v1

Figure S3.

doi.org/10.6084/m9.figshare.7881143.v1

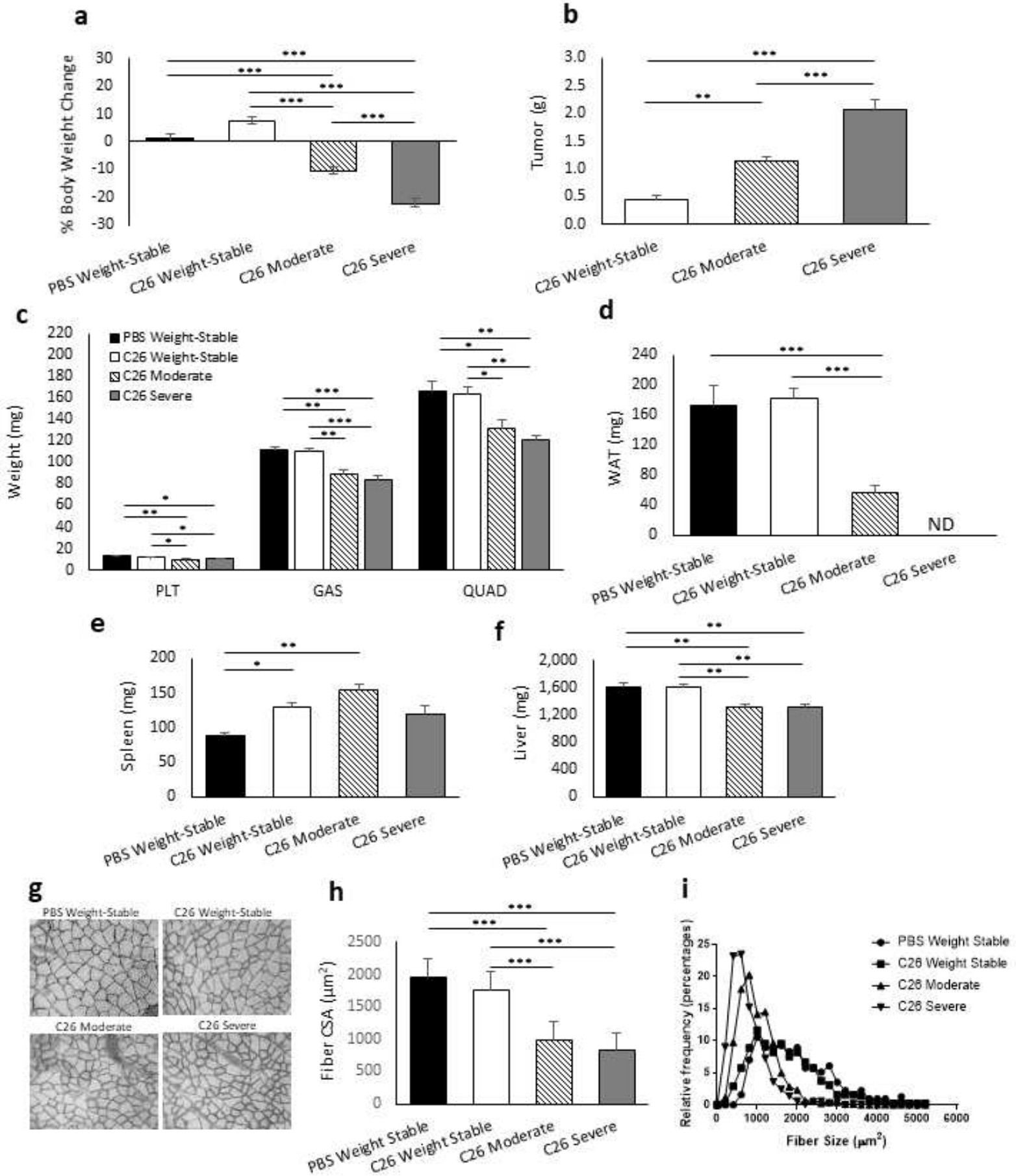
a
% Body Weight Change
30
20
10
0
-10
-20
-30
***
PBS Weight-Stable
C26 Weight-Stable
C26 Moderate
C26 Severe
b
Tumor (g)
3.0
2.5
2.0
1.5
1.0
0.5
0.0
**
***
C26 Weight-Stable
C26 Moderate
C26 Severe
c
Weight (mg)
PBS Weight-Stable
C26 Weight-Stable
C26 Moderate
C26 Severe
PLT
GAS
QUAD
d
WAT (mg)
ND
e
Spleen (mg)
f
Liver (mg)
g
h
Fiber CSA (μm²)
i
Relative frequency (percentages)
Fiber Size (μm²)

Figure 1

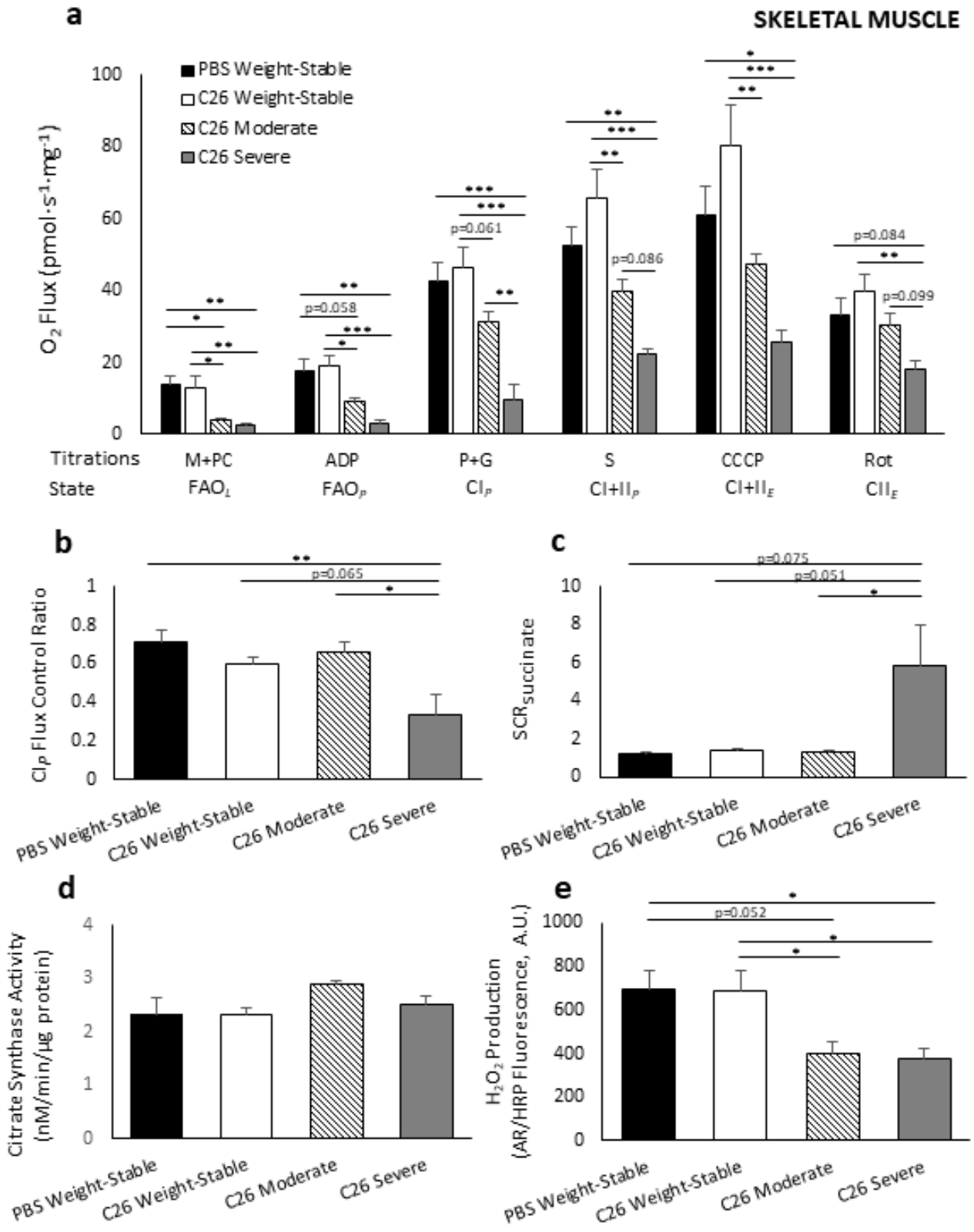
a
SKELETAL MUSCLE
PBS Weight-Stable
C26 Weight-Stable
C26 Moderate
C26 Severe
O2 Flux (pmol·s-1·mg-1)
Titrations
State
M+PC
ADP
P+G
S
CCCP
Rot
FAOL
FAOP
CIP
CI+IIP
CI+IIE
CIIE
p=0.058
p=0.061
p=0.086
p=0.084
p=0.099
b
CIP Flux Control Ratio
p=0.065
c
SCRsuccinate
p=0.075
p=0.051
d
Citrate Synthase Activity (nM/min/µg protein)
e
H2O2 Production (AR/HRP Fluorescence, A.U.)
p=0.052
PBS Weight-Stable
C26 Weight-Stable
C26 Moderate
C26 Severe

Figure 2

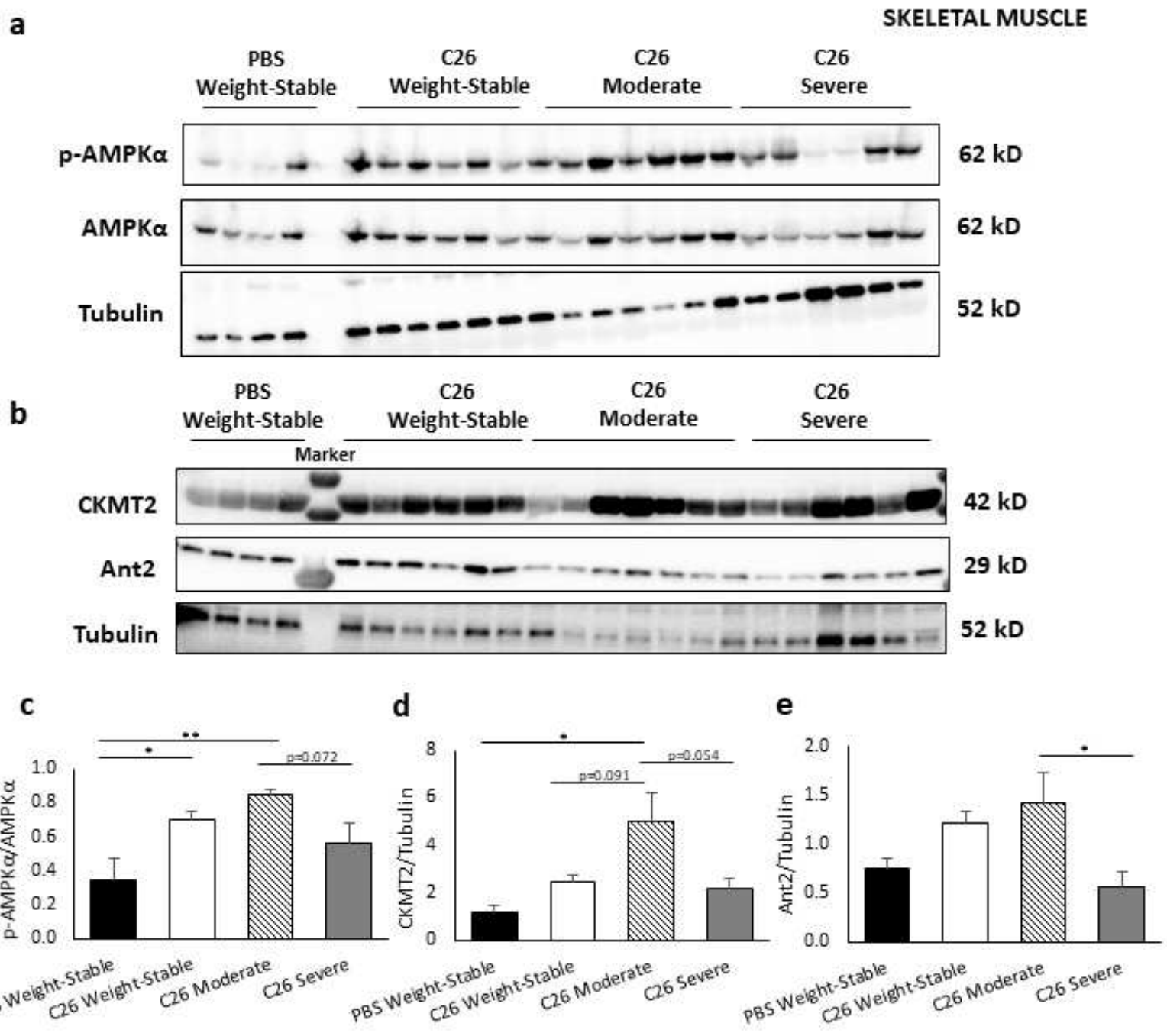
a
SKELETAL MUSCLE
PBS Weight-Stable
C26 Weight-Stable
C26 Moderate
C26 Severe
p-AMPKα
AMPKα
Tubulin
62 kD
62 kD
52 kD
b
PBS Weight-Stable
C26 Weight-Stable
C26 Moderate
C26 Severe
Marker
CKMT2
Ant2
Tubulin
42 kD
29 kD
52 kD
c
p-AMPKα/AMPKα
p=0.072
d
CKMT2/Tubulin
p=0.091
p=0.054
e
Ant2/Tubulin
PBS Weight-Stable
C26 Weight-Stable
C26 Moderate
C26 Severe

Figure 3

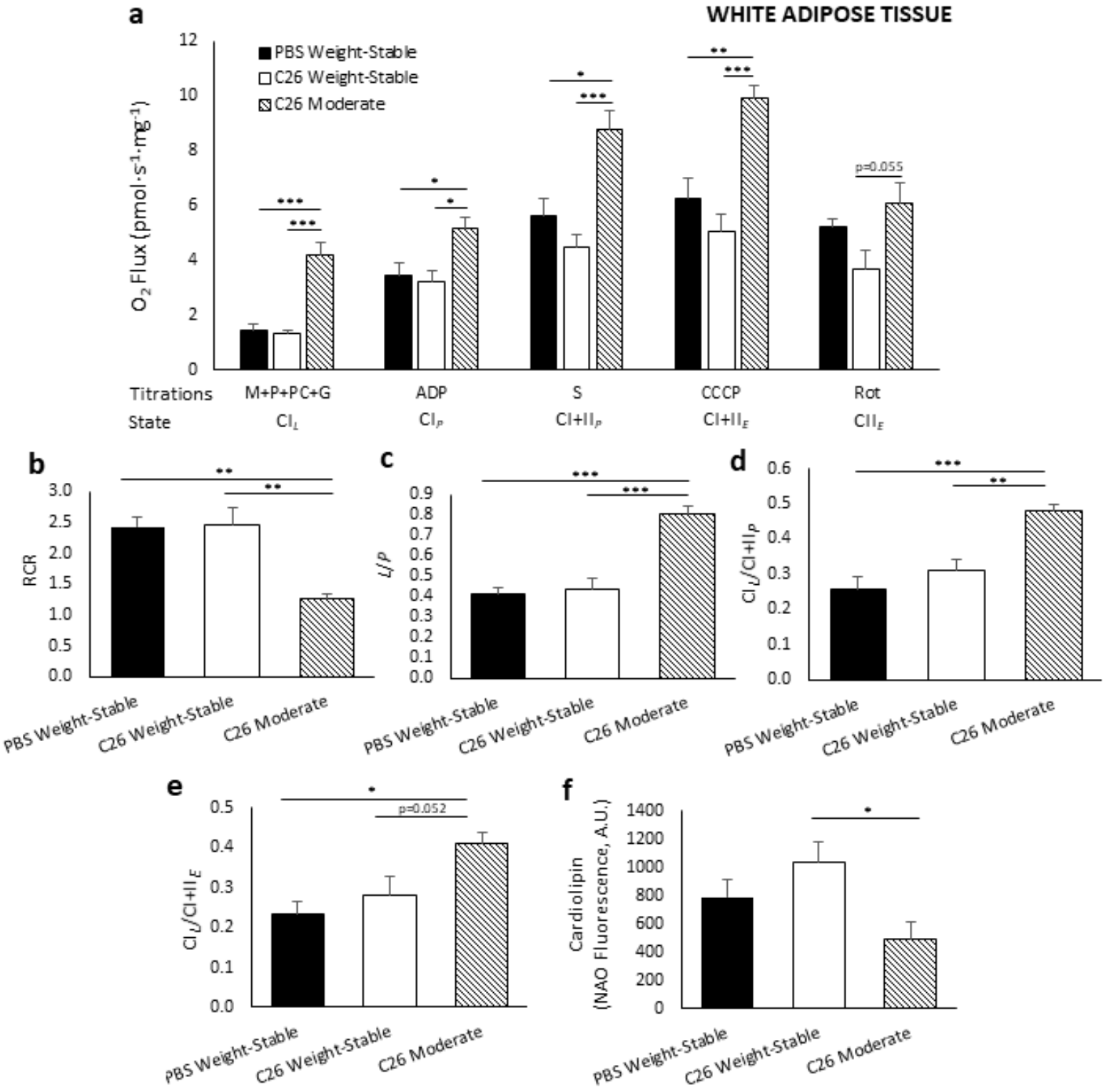
a
WHITE ADIPOSE TISSUE
PBS Weight-Stable
C26 Weight-Stable
C26 Moderate
O2 Flux (pmol·s-1·mg-1)
p=0.055
Titrations
M+P+PC+G
ADP
S
CCCP
Rot
State
CIL
CIP
CI+IIP
CI+IIE
CIIE
b
RCR
c
L/P
d
CIL/CI+IIP
e
CIL/CI+IIE
p=0.052
f
Cardiolipin
(NAO Fluorescence, A.U.)

Figure 4

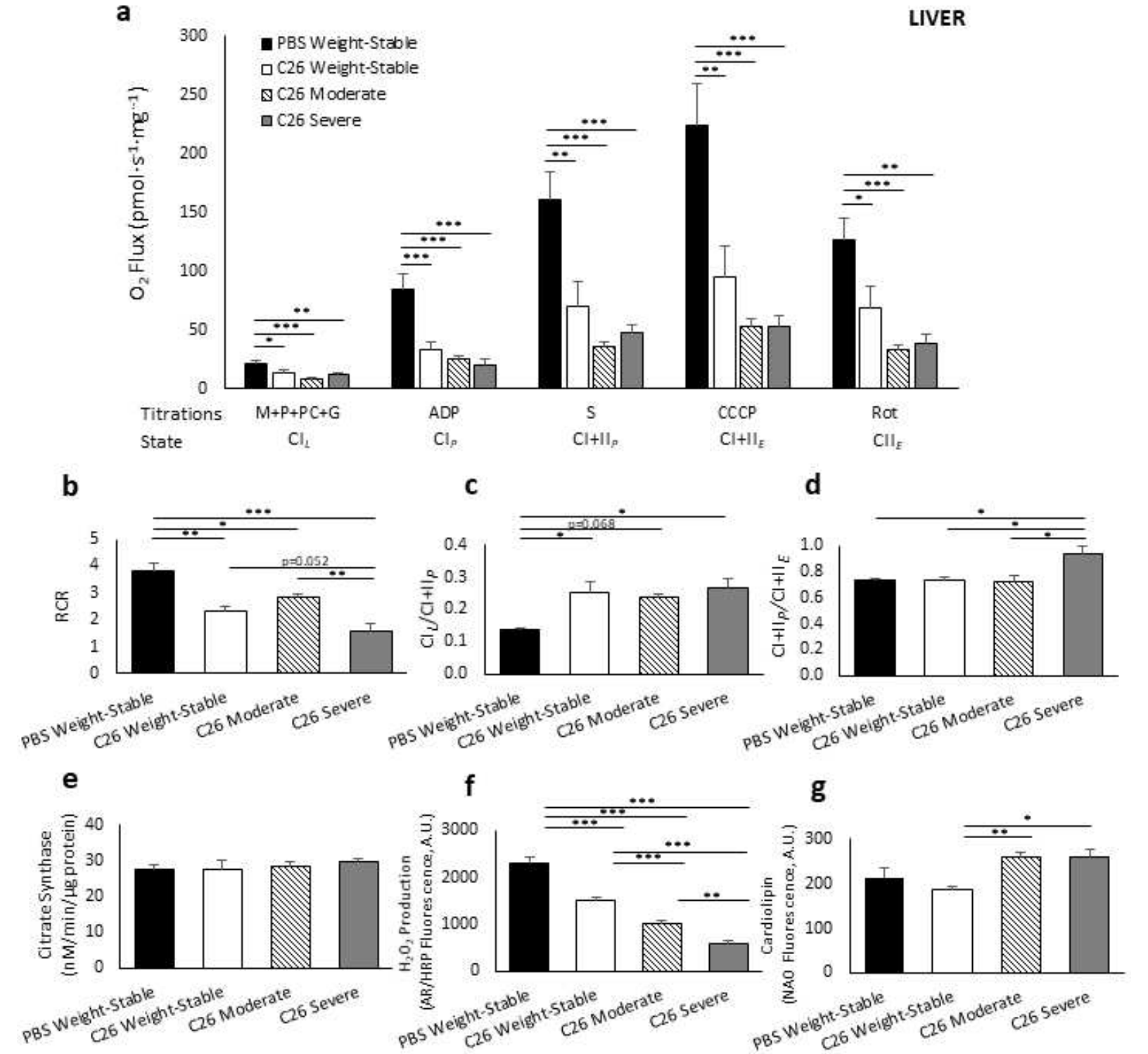
a
LIVER
PBS Weight-Stable
C26 Weight-Stable
C26 Moderate
C26 Severe
O2 Flux (pmol·s-1·mg-1)
Titrations
State
M+P+PC+G
ADP
S
CCCP
Rot
b
RCR
p=0.052
c
p=0.068
d
e
Citrate Synthase (nM/min/µg protein)
f
H2O2 Production (AR/HRP Fluorescence, A.U.)
g
Cardiolipin (NAO Fluorescence, A.U.)

Figure 5

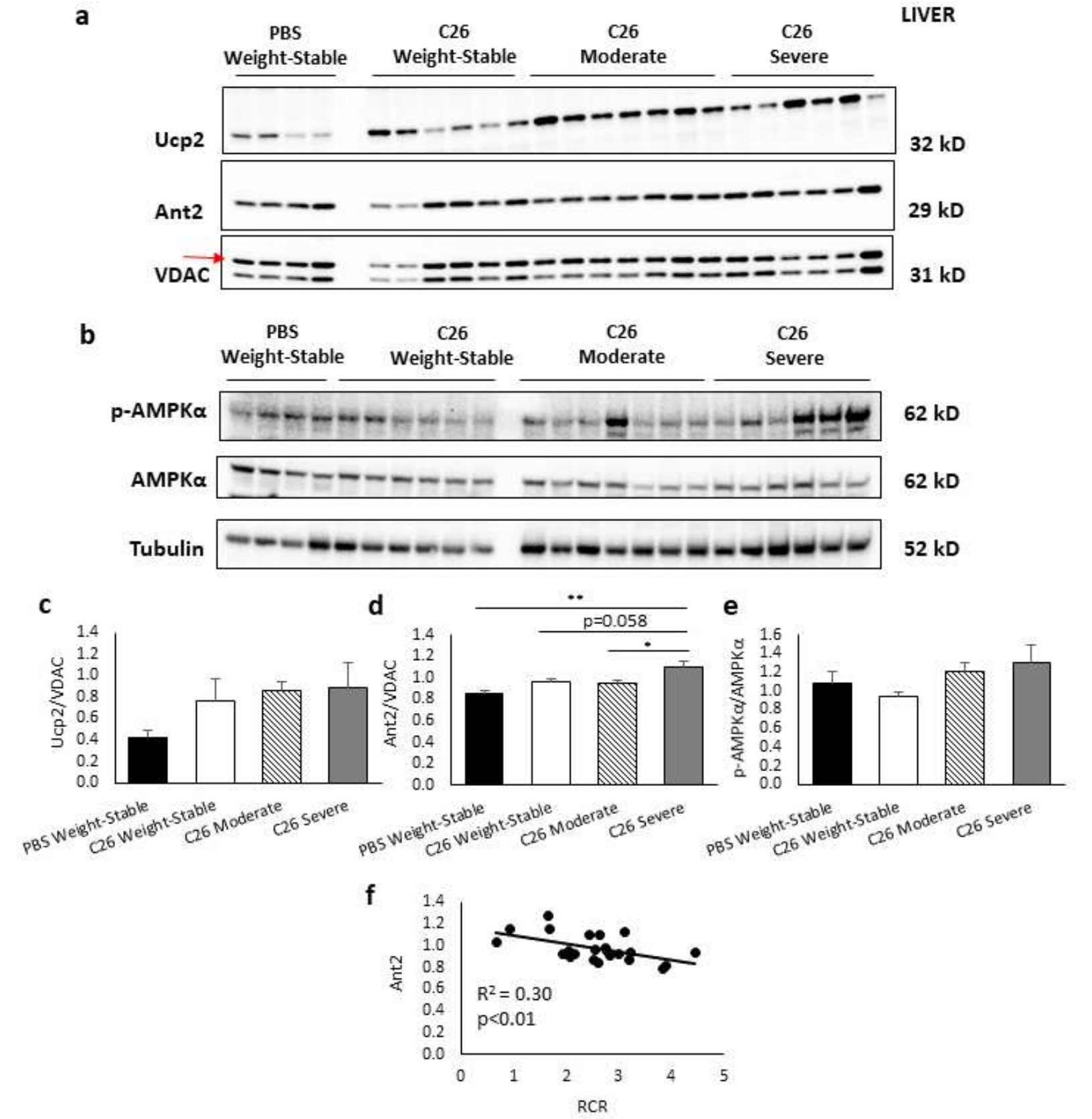
a
LIVER
PBS Weight-Stable
C26 Weight-Stable
C26 Moderate
C26 Severe
Ucp2
Ant2
VDAC
32 kD
29 kD
31 kD
b
PBS Weight-Stable
C26 Weight-Stable
C26 Moderate
C26 Severe
p-AMPKα
AMPKα
Tubulin
62 kD
62 kD
52 kD
c
Ucp2/VDAC
d
Ant2/VDAC
p=0.058
e
p-AMPKα/AMPKα
PBS Weight-Stable
C26 Weight-Stable
C26 Moderate
C26 Severe
f
Ant2
R² = 0.30
p<0.01
RCR

Figure 6

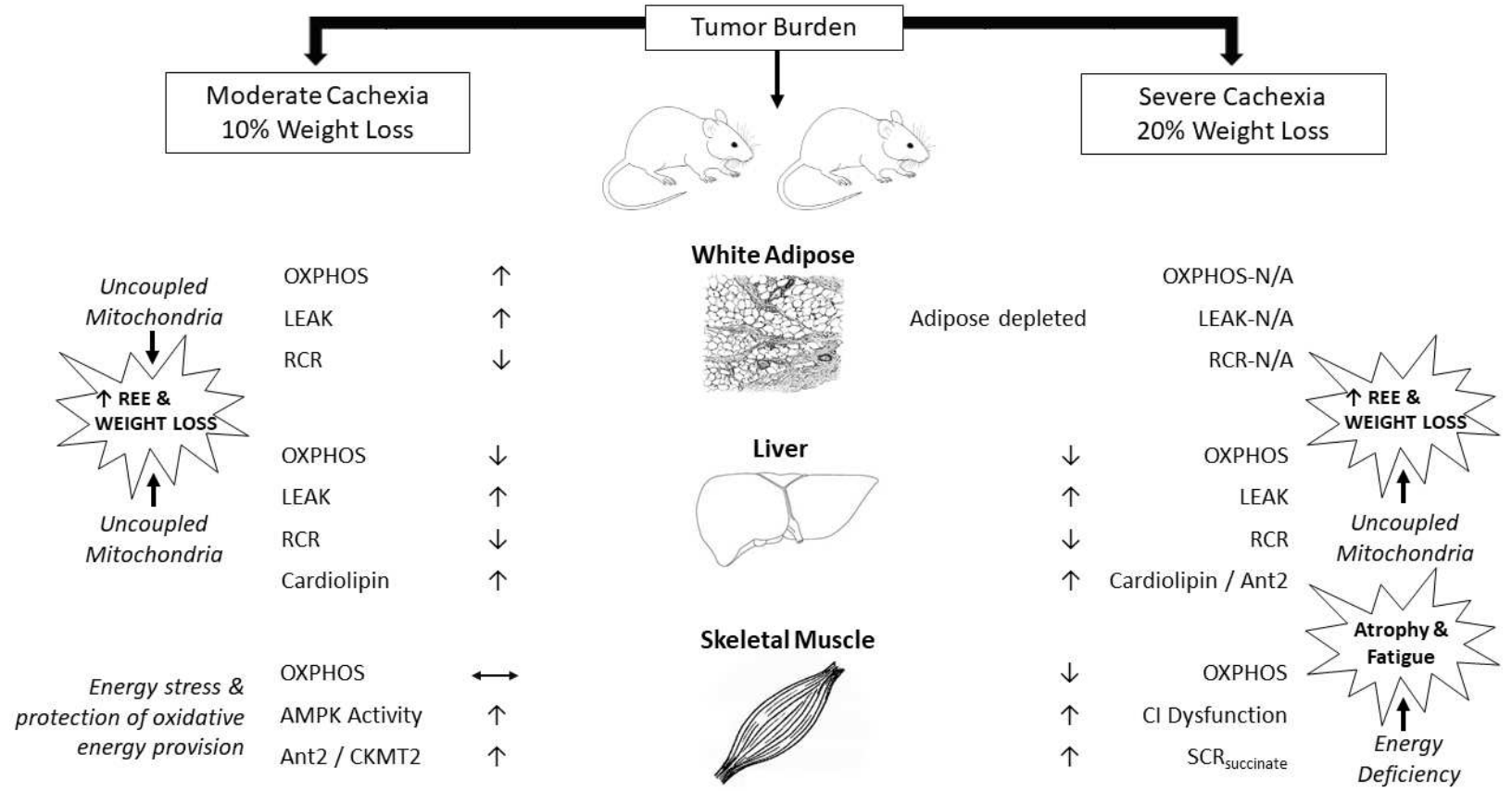
Tumor Burden
Moderate Cachexia
10% Weight Loss
Severe Cachexia
20% Weight Loss
White Adipose
OXPHOS ↑
LEAK ↑
RCR ↓
OXPHOS-N/A
Adipose depleted
LEAK-N/A
RCR-N/A
Uncoupled Mitochondria
↑ REE & WEIGHT LOSS
Liver
OXPHOS ↓
LEAK ↑
RCR ↓
Cardiolipin ↑
OXPHOS ↓
LEAK ↑
RCR ↓
Cardiolipin / Ant2 ↑
Uncoupled Mitochondria
↑ REE & WEIGHT LOSS
Skeletal Muscle
Energy stress & protection of oxidative energy provision
OXPHOS ↔
AMPK Activity ↑
Ant2 / CKMT2 ↑
OXPHOS ↓
CI Dysfunction ↑
SCR succinate ↑
Atrophy & Fatigue
Energy Deficiency